U.S. DEPARTMENT OF
ENERGY

Office of
**ENERGY EFFICIENCY &
RENEWABLE ENERGY**

Evaluation of the Reliability of Passive Infrared (PIR) Occupancy Sensors for Residential Indoor Lighting

U.S. Department of Energy—Lighting R&D Program

March 2022

Disclaimer

This work was prepared as an account of work sponsored by an agency of the United States Government. Neither the United States Government nor any agency thereof, nor any of their employees, nor any of their contractors, subcontractors or their employees, makes any warranty, express or implied, or assumes any legal liability or responsibility for the accuracy, completeness, or any third party's use or the results of such use of any information, apparatus, product, or process disclosed, or represents that its use would not infringe privately owned rights. Reference herein to any specific commercial product, process, or service by trade name, trademark, manufacturer, or otherwise, does not necessarily constitute or imply its endorsement, recommendation, or favoring by the United States Government or any agency thereof or its contractors or subcontractors. The views and opinions of authors expressed herein do not necessarily state or reflect those of the United States Government or any agency thereof, its contractors or subcontractors.

Authors

The authors of this report are all from RTI International:

J. Lynn Davis

Kelley Rountree

Andrew Dart

Clint Clayton

Roger Pope

Abdul Wallace

Meghan Hegarty-Craver

Acknowledgments

List of Acronyms

°C	degree Celsius
°F	degree Fahrenheit
μm	micrometer
55OL	operating lifetime tests conducted at 55°C
A	amp
ac	alternating current
Ah	amp-hour
ANOVA	analysis of variance
ANSI	American National Standards Institute
app	application
AST	accelerated stress test
AWG	American Wire Gauge
CSTA	continuous sensor triggering apparatus
CV	coefficient of variation
dc	direct current
DLC	Design Lights Consortium
DLT	detection length test
DOE	U.S. Department of Energy
DUT	device under test
EERE	Office of Energy Efficiency and Renewable Energy
EMS	Energy Management System
FOV	field of view
ft	feet, foot
ft/s	feet per second
GHz	gigahertz
hr, hrs	hour, hours
IES	Illuminating Engineering Society
IR	infrared

lbs	pounds
LCS	lighting control system
LED	light-emitting diode
lm/W	lumens per watt
MESA	Mission Execution and Strategic Analysis
MHz	megahertz
min	minute, minutes
mm	millimeter
NEMA	National Electrical Manufacturers Association
NETL	National Energy Technology Laboratory
OS-1	Occupancy Sensor Number 1
OS-2	Occupancy Sensor Number 2
PCB	printed circuit board
PE	polyethylene
PIR	passive infrared
PZT	lead zirconate titanate
RH	relative humidity
RoboSES	Robotic Sensor Evaluation System
RTOL	room temperature operating life
s	second, seconds
SSL	solid-state lighting
TE	thermoelectric
TO-5	Transistor Outline Package Number 5
UV	ultraviolet
V	volt
V_{dc}	direct current volt
W	watt
WAI	wireless–air interface

Executive Summary

Solid-state lighting (SSL) technologies have penetrated the general illumination market in recent years, largely replacing conventional technologies such as incandescent and fluorescent lighting. Most of the initial excitement about light-emitting diode (LED) sources for SSL devices focused on their energy savings potential resulting from vast improvements in source efficiency and luminous efficacy compared with conventional illumination products. More recently, the focus has shifted toward other aspects of lighting application efficiency, namely intensity effectiveness and spectral efficiency, because of the ease of controlling both the light intensity of LEDs with drive voltage and the color properties of the LED-based illuminators. To capitalize on the energy savings of increased intensity effectiveness and spectral efficiency, a lighting control system (LCS) is often used. While the current penetration of LCSs is relatively modest, it is anticipated that lighting controls (i.e., connected lighting, controls and LED and conventional lighting) could have an installed penetration as higher as 46% by the year 2035, saving an additional 1.3 quads of energy [1].

Despite the large energy savings that can be gained from using LCSs, standard test methods for evaluating sensors employed in LCSs and reliability data of the LCSs and their components are generally lacking. The National Electrical Manufacturers Association (NEMA) developed the only standard, NEMA WD 7-2011 (R2016), to test occupancy and motion sensor performance (herein referred to as "the NEMA protocol"). In a previous U.S. Department of Energy (DOE) effort, some concerns of the NEMA protocol were identified (e.g., strict height and weight limits on test subjects, large amounts of manual effort, sometimes inconsistent repeatability). During the current work, a consistent detection length test (DLT) and a Robotic Sensor Evaluation System (RoboSES) were developed to alleviate some of these concerns. RoboSES acts as a human surrogate by using thermal pads on a mannequin and a remote-controlled mobile base to test a sensor's field of view (FOV).

This report builds on the earlier DOE efforts to understand sensor technologies used in LCSs for general illumination. Specifically, this report describes the optimization of RoboSES, characterizes and establishes test methods to assess the reliability of multiple passive infrared (PIR) sensors, and reports the findings of robustness and reliability testing on two commercial PIR sensors intended for residential applications. The information presented in this report is gained from up to 4,000 hours (hrs) of accelerated stress tests (ASTs).

The commercial PIR sensors covered in this report are referred to as Occupancy Sensor Number 1 (OS-1) and Occupancy Sensor Number 2 (OS-2). The first product (i.e., OS-1) is part of a home automation system consisting of an Internet bridge, an A19 lamp with smart capability (i.e., switching, dimming), and a sensor that contained both a PIR detector (for occupancy) and a photocell (for light intensity). The second product (i.e., OS-2) is part of a different home automation system that consisted of a proprietary Internet hub, a wireless smart switch, a different A19 lamp (i.e., one without smart capability), and a motion-only occupancy sensor. Both OS-1 and OS-2 use a PIR detector in a Transistor Outline Package Number 5 (TO-5), contain a Fresnel lens, and can be programmed through a proprietary application (app) hosted on a mobile phone or other supported device. OS-1 used a low-power radio transceiver (2.4 gigahertz [GHz]) to communicate with the controller, whereas OS-2 used a loop antenna for short-range communication at 908 megahertz (MHz).

This current report presents findings of the ASTs of OS-1 and OS-2 PIR sensor device under test (DUT) populations through 4,000 hrs of exposure to a continuous room temperature operating life (RTOL) test and a continuous operating life test in an elevated temperature environment of 55 degrees Celsius (°C) (55OL). This current report also discusses the findings of a rapid triggering AST through 2,000 hrs. During the rapid triggering test, sample populations of OS-1 and OS-2 were continually activated every 90 seconds (s). The PIR sensor populations in both RTOL and 55OL were continuously on, but not triggered.

The reliability findings in this report for OS-1 and OS-2 reflect only the sensors themselves and not the entire LCS. The decision to evaluate only the sensors was made because, when testing according to the NEMA protocol, system latency issues with the LCS caused repeatability concerns of when and which cell was

occupied by the test subject when the sensor was triggered. However, OS-1 and OS-2 had LED indicators on the front of the sensors to instantaneously show motion detection, and this removed the need for the remainder of the LCS during the tests described in this report.

To optimize RoboSES and track performance of the DUTs, a DLT was developed. The DLT served as a simple measurement of the maximum distance at which the PIR sensor could detect the test subject. In the DLT, the test subject (i.e., a human or RoboSES) would walk into the FOV of the sensor from the side (i.e., parallel to the surface of the sensor) beginning in 3-foot (ft) increments at a distance outside the FOV of the sensor. If the sensor was not triggered, then the test subject would step 3 ft closer and repeat the test. After 4,000 hrs of exposure to RTOL or 55OL or 2,000 hrs of exposure to the rapid triggering test, all test populations of OS-1 and OS-2 DUTs showed no significant change in detection distance by the DLT. This finding suggests that the sensors have good robustness, at least when it comes to maximum detection length.

FOV testing was performed in a large, open conference room using human test subjects, and the test procedures followed the NEMA protocol (except for height and weight requirements on some test subject during the initial testing). The sensors were measured when they were new (i.e., initial measurement) and again at the end of the various ASTs, and the measurements only covered one active quadrant. The sensors were set up in an array so that testing of multiple sensors at one time was possible. The area of the FOV was calculated by the number of 3-ft × 3-ft cells where motion was detected. A one-factor analysis of variance (ANOVA) was conducted on the population averages for OS-1 and OS-2 under the four test conditions (i.e., initial; 4,000 hrs of RTOL; 4,000 hrs of 55OL; and 2,000 hrs of rapid trigger). The ANOVA findings revealed that no statistically significant differences in the means between the four populations of either OS-1 ($p = 0.416$) or OS-2 ($p = 0.181$) were found. The coefficient of variation (CV) of the number of active cells was found to be small (<5%) for all test populations of OS-1, but up to 21.5% for OS-2.

The small CV for OS-1 was accompanied by relatively uniform FOV across sensors, suggesting that the NEMA protocol provides a consistent and reliable measure for OS-1. Furthermore, the FOV results for OS-1 aligned with the DLT results and suggested that there was no statistically significant change in FOV for OS-1 after the different AST environments. However, the large CV and wide part-to-part variability in FOV uniformity demonstrated by OS-2 suggest that the NEMA protocol might not provide consistent results for these sensors. Therefore, any small changes because of AST would be practically impossible to identify.

The findings presented in this study highlight the importance of a reliable test method to assess sensor performance. As a workaround to LCS latency, only the reliability of the sensors themselves was studied. A DLT was developed as a quick check of sensor performance, and sensors were arrayed so that the more intensive FOV testing via the NEMA protocol could be completed in a reasonable amount of time. The results of the DLT and FOV tests suggest that the sensors studied and discussed in this report are robust to indoor stressors. Further operation time in AST or higher AST environmental stressors are needed to assess possible degradation or failure mechanisms.

Table of Contents

List of Figures

List of Tables

1 Introduction

1.1 The Role of Sensors in Lighting Systems

Solid-state lighting (SSL) technologies have utilized high efficiency, light-emitting diodes (LEDs) with great effectiveness to reduce the energy consumption associated with lighting. As a result of the higher efficiencies and low carbon footprint, SSL technologies are displacing more energy intensive conventional lighting technologies (e.g., incandescent, fluorescent, high-intensity discharges) in practically all lighting applications. The degree to which SSL technologies have penetrated traditional lighting markets varies by application. In 2020, the total stock penetration of SSL technologies in the United States ranged from 29% for industrial lighting to 66% for outdoor lighting [1]. By converting to more efficient SSL technologies, the energy consumption attributable to lighting was reduced by 1.1 quads in 2017, when the total market penetration was only 19%. In 2035, it is estimated that SSL technologies will constitute 84% of all unit installations in the United States, resulting in an annual primary energy savings of 4.8 quads compared with conventional lighting technologies [1, 2].

Although the efficiency gains that have been achieved with SSL technologies are impressive, LED-based lighting technology offers another benefit that is not as widely utilized—SSL devices are generally compatible with control technologies that can further reduce energy consumption. Specifically, the inherent properties of LED sources, such as instant on, easy dimmability, and rapid response to control signals, make this technology more amenable to lighting controls than many conventional sources. Therefore, in addition to the energy savings that can be achieved by more efficient SSL technologies, the addition of controls also offers the potential for even greater energy savings.

Sensors and control systems used in general illumination application can be classified as those that control lighting power levels (e.g., dimming, daylight harvesting), those that automatically turn the lights on and off based on the presence or absence of people (e.g., occupancy sensors, timers, motion sensors), and those that adjust the light color in a tunable system (e.g., chromaticity sensors). As described in a report of findings from a U.S. Department of Energy (DOE) [1], the penetration of sensors and controls was found to be lagging that of SSL devices. The study found that 66% of commercial buildings and 86% of residential buildings did not have any controls for their lighting systems. Out of the 34% of the commercial spaces that did have controls, almost half of those (47%) had an Energy Management System (EMS) as the dominant lighting control technology, and an additional 18% utilized occupancy sensors often in conjunction with an EMS [1]. An EMS is a computer-based system that uses multiple inputs (e.g., time of day, building use profiles, occupancy) to control energy. Typically, the EMS controls operation of the building's lighting and heating, ventilation, and air conditioning systems, and energy use can be timed to periods of high building occupancy and cutback during off-hours. Of the 14% of residential buildings with some form of controls, the dominant lighting control technology was a simple dimmer, which was present in 79% of these homes [1]. Other lighting control technologies were found to have a minor presence in residences for 2017 but that could be changing with the rise of smart technologies for residential applications. Overall, only 19% of all lighting installations in the United States used some form of controls in 2017; however, this number is projected to be as high as 46% of all lighting installations by 2035, with the largest gains in lighting control technology occurring with LED devices [1].

The main sensor technologies used in lighting control systems (LCSs) can be broadly divided into those that control the electrical power being fed to the lights (e.g., dimming, daylight harvesting) and those that reduce the operating hours of the lights when not needed (e.g., occupancy sensors, timers). The global occupancy sensor market is projected to be $1.7 billion in 2022 and is expected to increase to $4.8 billion by 2028 (18% compound annual growth rate) [3]. Most of this increase in product demand is driven by a desire to conserve energy and reduce carbon emissions by improving the energy efficiency of commercial buildings and private residences. North America is the largest market for occupancy sensors, accounting for 39% of the total occupancy sensor market. Europe is currently the second largest market with Asia-Pacific the third largest;

however, the compounded annual growth rate of occupancy sensors is the largest in Asia-Pacific (15.1%) due primarily to increased adoption in China.

Sensors used to detect occupancy generally utilize one of three technologies: passive infrared (PIR), ultrasound waves, or microwaves [4–6]. The PIR technology is by far the dominant approach currently used to detect occupancy and accounts for approximately 77% of the occupancy sensor market in 2019. The growth of the residential occupancy and motion sensor market has been aided in part by the low cost and low power requirements of PIR sensors. Therefore, PIR sensors can be expected to have a significant presence in the occupancy sensor market in the foreseeable future. For this report, an "occupancy sensor" is defined as an indoor sensor that automatically turns the lights on when a space is occupied and automatically turns the lights off when no movement is detected. In contrast, a "motion sensor" is defined as an outdoor sensor that automatically turns the lights on when motion is detected and automatically turns the lights off when no movement is detected. Both occupancy and motion sensors use PIR detectors, although the way that the electronics in the sensor process the PIR output is slightly different between the two. In addition, a dual-mode sensor can be created by combining two or more sensing modalities (e.g., PIR, ultrasonic) to reduce the likelihood of any false positives or false negatives [6]. Advanced data processing techniques are also possible with PIR sensors to improve accuracy [7].

A PIR detector uses a Fresnel lens, typically made from polyethylene (PE), to form multiple discrete fields of view (FOVs) that are strategically located throughout a coverage area. Thermal energy produced by a person moving through the sensor's FOV are collected by at least one lenslet of the Fresnel lens and focused onto a pyroelectric sensing element [4, 5]. A "pyroelectric material" is a crystalline material that generates a temporary voltage that is proportional to the rate of heating or cooling, which causes a temporary change in the polarization of the crystal lattice of the pyroelectric materials. Two examples of common pyroelectrical materials are lead zirconate titanate (PZT) and barium titanate.

Because the pyroelectric response is at a maximum when the temperature suddenly changes and gradually decreases as the material reaches thermal equilibrium, a pyroelectric sensor is good at detecting the entrance and exit of a heat source as it passes through the sensor's FOV if the heat source is at a different temperature than the thermal background. Heat sources such as a person who does not change his or her location while in the sensor's FOV will result in a diminishing signal from the PIR detector. When the person moves between Fresnel lenslets, the image will change on the PIR sensor, thus initiating a sharp sensor response. When a heat source activates the PIR sensor, a timer in the sensor's circuitry starts; the timer is set to indicate the length of time that the lights will remain on after the last movement of a heat source has been detected. If motion is detected during this interval, then the timer restarts. If motion is not detected during this interval, then the sensor will turn off the lights at the end of the time interval.

Pyroelectric elements have a polarity and are connected serially with reverse polarity (e.g., the negative terminal of one element is connected to the negative terminal of the next element). Typically, there are either two or four pyroelectric elements in a PIR sensor. The two-element version is commonly used in wall sensors, and the more sensitive four-element version is commonly used in ceiling-mounted sensors. PIR sensors are termed as "passive" because they do not radiate infrared (IR) energy; instead, they only detect IR energy. The pyroelectric elements used in PIR sensors typically have a high-pass filter before the pyroelectric element to block radiation with wavelengths below 5 micrometers (μm). This passband matches well with the thermal emissions from the human body; these thermal emissions typically have a maximum occurring over the wavelength range from 8 to 14 μm [4, 7]. Parameters that impact the sensitivity of PIR sensors include the distance of the object from the detector (emission power varies as $1/[\text{distance}]^2$), the difference in temperature between the object and the background, the rate of movement of the object, the transmissivity of the Fresnel lens (dependent upon thickness and shape), and the response of the pyroelectric elements and associated electronics.

1.2 Challenges in Sensor Evaluation

Although sensors are a critical part of the energy savings potential of LED lighting systems, standard test protocols for evaluating sensors used in LCSs are generally lacking. For example, no recognized consensus-based standards currently exist for measuring occupancy sensors; therefore, this may contribute to the lagging market penetration of sensor technologies [6]. The main test protocol that is available for use by the industry is one that was developed by equipment manufacturers and is part of the National Electrical Manufacturers Association (NEMA). This test protocol for occupancy and motion sensors was published as the only standard, NEMA standards publication WD 7-2011 (R2016) [8], which is henceforth referred to as "the NEMA protocol" in the remainder of this report. Although this protocol is the only available technique for testing sensor performance, there are limitations with using it, as discussed in Section 4 of an earlier DOE report [6].

Performing reliability studies of PIR sensors requires conducting tests on the initial performance of the devices under test (DUTs) and subsequent performance tests after aging usually performed under accelerated conditions. Benchmarking the initial performance of an occupancy sensor may require evaluating a sensor's range, FOV, response time, latency, and ability to handle obstacles such as walls. Such information would provide a basis for comparing the initial performance of a sensor with performance after aging. Testing the reliability of a lighting sensor involves evaluating the temporal changes of all these properties or a subset of the most critical properties, such as range and FOV, that are judged to be the best proxies for long-term performance. Ideally, tests that are used in sensor reliability studies to measure changes in sensor performance over time should be reproducible, easy to perform, and low cost.

A primary approach for measuring the performance of occupancy sensors when detection distance is an important parameter is to move the target with respect to a sensor positioned at a fixed location. This method can be used for PIR sensors and for active sensors such as ultrasonic and microwave devices. When using the NEMA protocol, measuring sensor performance is accomplished by a human moving at a brisk pace throughout the sensor's FOV, as shown in **Figure 1-1**, and then measuring where in the sensor's FOV that motion was detected. The sensor is continuously powered during use but is only triggered (i.e., detects movement) when the test subject moves across the sensor's FOV and imaged on the detector. In addition to humans, a robot or other mechanical structure can be used as the test subject, provided that the robot has a size and thermal profile similar to a human. The heat signature can be produced in several different ways by using electrical heaters or another source of heat above ambient levels.
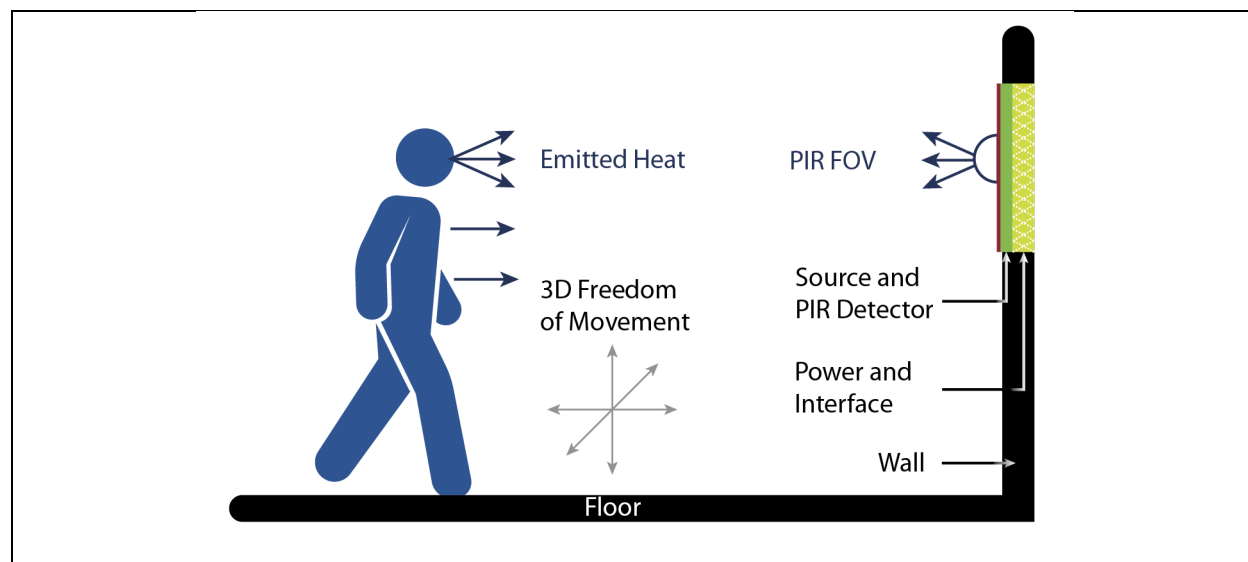

Figure 1-1. A schematic of a test setup for a passive sensor such as a PIR device

This current report focuses on reliability testing of occupancy sensors from typical systems that can be purchased at big box retailers and are intended for use in residential smart houses. This analysis examines different operating temperatures as environmental stressors that could compress the lifetime of occupancy sensors and provide insights into possible failure modes. This report presents the findings through 4,000 hours (hrs) of continuous operating testing at room temperature and in an ambient environment of 55 degrees Celsius (°C). Although these DUTs are continuously powered during the operating test, they are not consistently triggered because of the difficulties associated with detecting motion in an enclosed environmental chamber. Therefore, as an additional test, the possibility of a rapid triggering test, during which each sensor detects motion once every 90 seconds (s), was explored. This report also provides data on the design and initial performance of a Robotic Sensor Evaluation System (RoboSES) as compared with human testing. Altogether, the current report demonstrates the importance of standardized and reproducible test methods in reliability studies and describes the types of information that such studies can provide for lighting technologies.

1.3   Metrics for Sensor Failure

When evaluating the reliability and lifetime of sensors, it is critical to examine the use case and determine what constitutes a failure. Sensors used in LCSs generally control energy use by turning luminaires and lamps on and off or by adjusting lighting levels. In general, the "reliability of a lighting system" can be defined as the ability to perform an intended function over a specified period and under specified use conditions. Based on this definition, the reliability of a sensor used in a lighting system can be measured by determining the likelihood that either an abrupt or parametric failure of the lighting system will occur because of an erroneous reading provided by the sensor. An "abrupt failure" can be defined as either a complete loss of function of the lighting system because of a sensor malfunction (i.e., the lights will not come on) or the loss of an expected function of the lighting system (e.g., dimming, daylight harvesting). One example of an abrupt failure is an inoperable sensor that prevents the lighting system from turning on. A parametric failure occurs when the lighting system still provides light, but the light does not have the intended properties because of a sensor malfunction. An example of a parametric failure would be a change in the FOV of a sensor so that it is only activated at a shorter distance than when first installed. Disabled sensors or poorly commissioned lighting systems are examples of human error; therefore, they are not discussed in this report.

To assess the reliability of occupancy sensors used in indoor systems, the FOV and detection distance can be used as key metrics. In addition, other metrics such as part-to-part variability and the reading tolerances of individual sensors can be useful in assessing the consistency of sensor response. Obviously, if a sensor is not working and does not produce a control voltage, then an abrupt failure has occurred. However, a parametric failure in the lighting system can also occur when a control sensor is operational but providing the wrong control voltages because of an incorrect reading (e.g., change in FOV, detection distance).

2   Sample and AST Descriptions

2.1   Sample Descriptions

For an examination of the reliability of low-cost, commercial occupancy sensors, two different occupancy sensor products that can be easily found at big box retailers or online were targeted. Both products are typically used in home automation and/or security systems to trigger events such as light automation or sounding an alarm. Operating the sensor network requires several electronic components: a controller (which can be either a hub or a bridge), smart switch nodes to active or deactivate an electrical light fixture, a means to connect to a mobile phone through a local network (e.g., WiFi, Bluetooth), and possibly an Internet connection. The controller connects and sends commands to nodes on the home networks (e.g., switches) based on sensor response and other inputs. Programming the home network is accomplished through a vendor-specific smartphone application (app) that interfaces with the controller by using a WiFi network. When using some smartphone apps, users can control their devices outside of their home network by employing the Internet accessed through a mobile telephony network or a different WiFi network. The controller communicates to the nodes on the network through a short-range radio wireless–air interface (WAI) such as Bluetooth, WiFi,

Zigbee, or Z-Wave. In this way, the response from an occupancy sensor can be used to carry out a command (e.g., turning a standard A19 lamp on and off through a wireless switch). A schematic of a typical network configuration is provided in **Figure 2-1.**
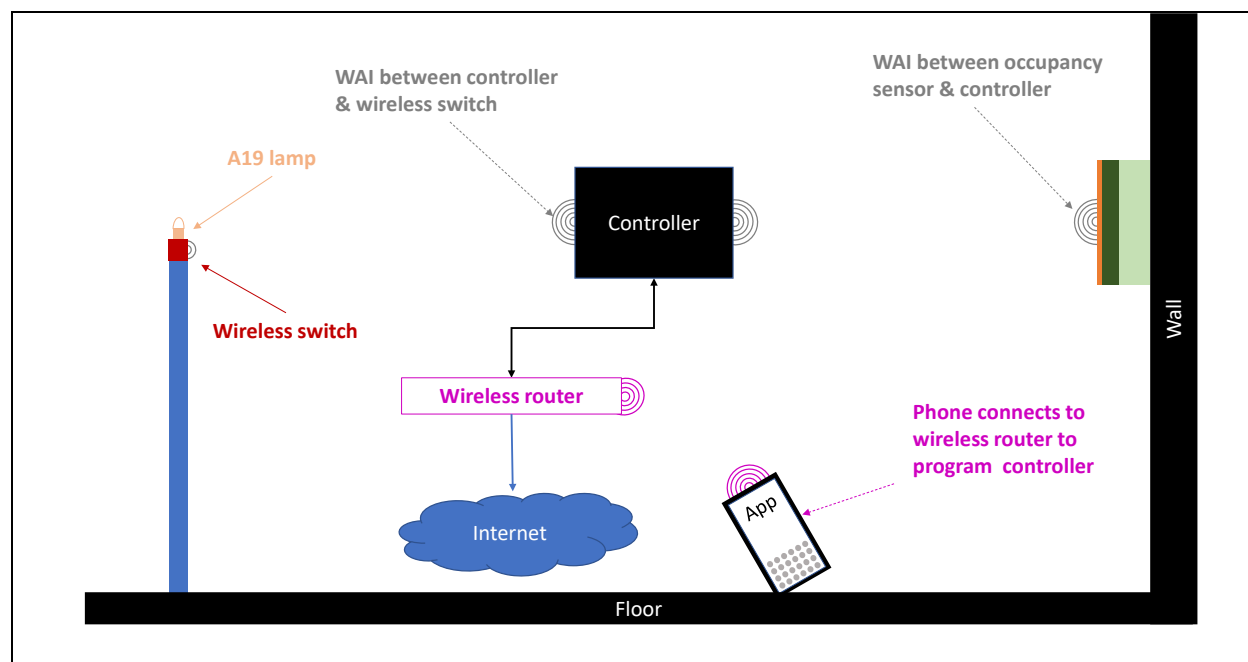
Figure 2-1. Schematic of a typical wireless network on a smart controller

The first product that was tested was part of a home automation system consisting of an Internet bridge, an A19 lamp with smart capability (i.e., switching, dimming), and a sensor that contained both a PIR detector (for occupancy) and a photocell (for light intensity). This first product is henceforth referred to as Occupancy Sensor Number 1 (OS-1) in this report; photographs of the sensor are shown in **Figure 2-2**. OS-1 was designed to be powered by two AA batteries, which reside on either side of the main printed circuit board (PCB). The use of primary batteries at elevated temperatures is known to cause issues with the performance, reliability, and safety of electrical devices. Therefore, in all testing described in this report, OS-1 DUTs were powered by an external power supply. This approach allowed the OS-1 DUTs to be tested at elevated temperatures without worrying about the impact of heat on battery operation.

Inside OS-1 is a PIR detector in a Transistor Outline Package Number 5 (TO-5) package, a photodiode, and a low-power radio transceiver operating at 2.4 gigahertz (GHz). The PIR detector has a high-pass optical filter built into the exterior of the TO-5 package to allow IR radiation above the passband to reach the pyroelectric element. The exterior of the PIR package is covered by a Fresnel lens made of PE; this lens is visible outside of the sensor. Programming the network consists of using a proprietary app hosted on a mobile phone or other compatible device to configure the system. Firmware for all connected products was updated as of June 9, 2021 to the latest version. The system could be programmed so that an A19 lamp (with built-in smart dimming and on and off switching) would turn on when the connected occupancy sensor detected movement and would turn off after 1 minute (min) when no motion was detected. Whenever the sensor detected motion, an indicator LED (see **Figure 2-1**) would turn on, and this signal was used to measure sensor response in all tests described in this report. As explained in **Section 3.2.1**, measuring sensor response through the indicator LED was found to be the fastest and most reproducible means of determining sensor activation.
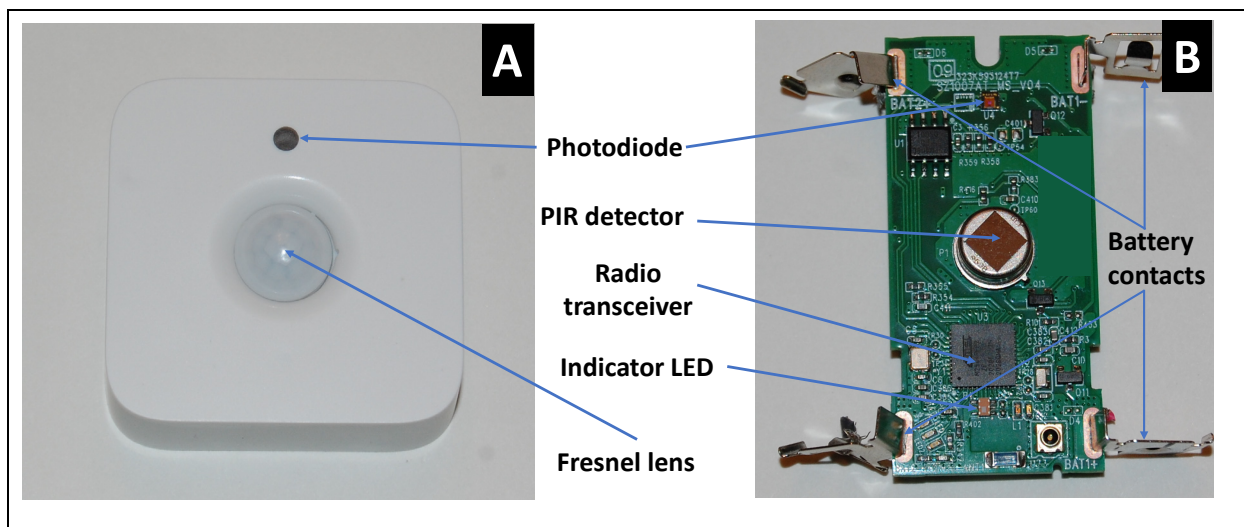
Figure 2-2. (A) The fully assembled OS-1, and (B) the sensor with the cover and Fresnel lens removed

The second product that was tested (i.e., Occupancy Sensor Number 2 [OS-2]) was from a different home automation system that consisted of a proprietary Internet hub, a wireless smart switch, a different A19 lamp (i.e., one without smart capability), and a motion-only occupancy sensor. OS-2 is powered by a CR123A lithium primary battery located in an external compartment of the sensor housing, and the voltage is provided to the main PCB through two connector pins that extend into the battery compartment. To eliminate any issues arising from battery performance and reliability, an external power supply was used in all testing of OS-2. A photograph of OS-2 is shown as **Figure 2-3**. The interior of this sensor consisted of a PIR detector in a TO-5 package with a long-pass filter built into the package, a status indicator LED, a Fresnel lens, a loop antenna for short-range communication at 908 megahertz (MHz), and a radio transceiver board (on the back of the PCB). Using a proprietary app hosted on a mobile phone, the test system could be configured so that the wireless switch would turn on an A19 lamp whenever the occupancy sensor was tripped, and the lamp would turn off after 1 min of no motion. Firmware for all connected products was updated as of June 9, 2021 to the latest version.
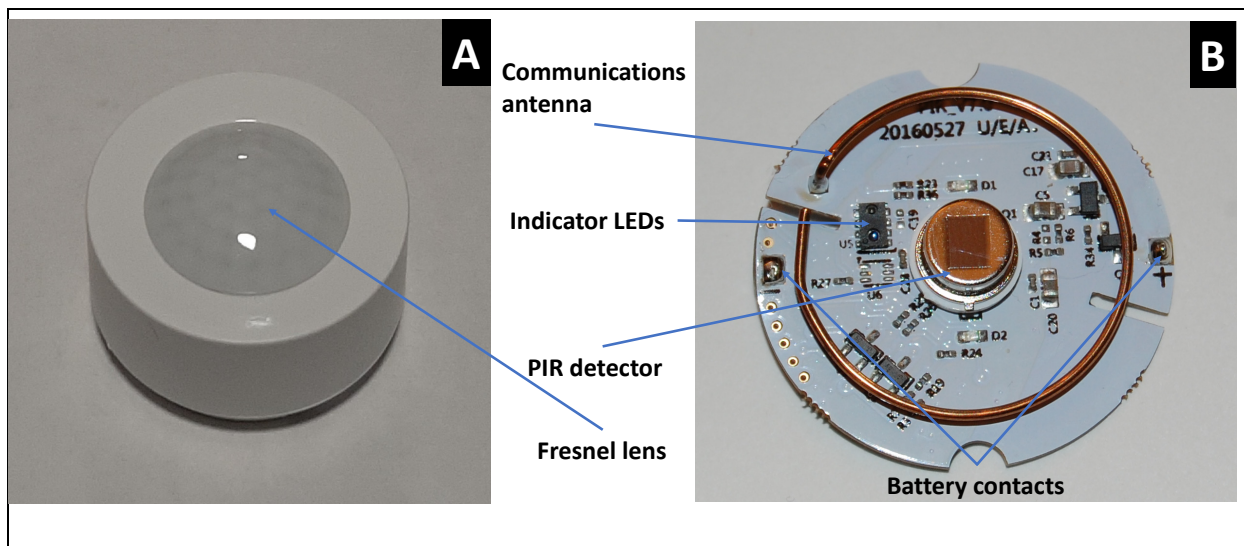

Figure 2-3. (A) The fully assembled OS-2, and (B) the sensor with the cover and Fresnel lens removed

2.2   Accelerated Stress Test Conditions

Most of the components used in the PIR sensors shown in **Figure 2-2** and **Figure 2-3** are relatively robust and can withstand short-term temperature excursions of 150°C or higher. The ability of the PCB components to withstand temperature excursions can be assumed because most components are surface mount designs that are reflow soldered. The main exception is the PIR sensor, which is a through-hole device in a TO-5 package where the leads are soldered to the PCB most likely through hand soldering to minimize the heat that the sensor experiences during PCB population. Another critical component of the PIR system is the Fresnel lens, which is typically made from PE, which has a relatively low heat deflection temperature. Because of the temperature sensitivity of the components of the PIR sensor (including the PE lens), manufacturers of PIR sensors typically set the upper usable ambient temperature at up to 60°C when such devices are energized [9, 10]. This usable ambient temperature sets the upper limit for any operating lifetime tests because exceeding this temperature may cause plastics (e.g., PE) to deform and may damage the pyroelectric element. This value is higher than the specified operating temperature of OS-1, which is 40°C. The exact reason for the low temperature specification of OS-1 is unknown, but it can be speculated that it may be because of the use of alkaline batteries to power the sensors. For example, the maximum usable ambient temperature of an alkaline battery is typically 54°C to 60°C [11–13].

During this study, lifetime tests were conducted at two temperatures: room temperature (i.e., 25°C) and 55°C. The room temperature operating life (RTOL) test was conducted on a benchtop at an ambient temperature of 24°C ± 2°C, whereas the operating life test conducted at 55°C (55OL) was performed in an oven set to 55°C. Different populations of OS-1 and OS-2 were used for RTOL and 55OL, with the sample size for each test being three DUTs for each product. The DUTs were evaluated after every 1,000 hrs of exposure, and performance was checked with a detection length test (DLT; see **Section 3.2.2**). During operating life testing, each DUT was powered by an external power supply through the battery contacts, and the cumulative operating time for each DUT under these conditions was limited to 4,000 hrs.

Another approach to test the reliability of a PIR occupancy sensor is to continually trigger the sensor and determine whether its response changes over time with continual triggering. To perform this test, the continuous sensor test apparatus (CSTA) was constructed (**Figure 2-4**). The CSTA consists of the sensor test plate and a thermal source mechanism. The sensor test plate contains locations where up to six different sensors could be mounted with each DUT powered by an electrical lead that extends through a hole in the metal substrate to an external power supply. The thermal source mechanism contains a 2-inch × 2-inch thermoelectric (TE) element that effectively serves as a black body thermal radiator for the purposes of this test. The TE was mounted on a heat sink (approximately 2 inches × 2 inches) and connected to an external power supply for operation. An electric shutter mechanism consisting of a polycarbonate plate attached to a rotating hub was mounted in front of the TE element to modulate the heat source. The electric shutter mechanism operated on a timer and could trigger each DUT on the sensor test plate with a period of 90 s. The sample size for each sensor for the triggering test was also three DUTs for each product.
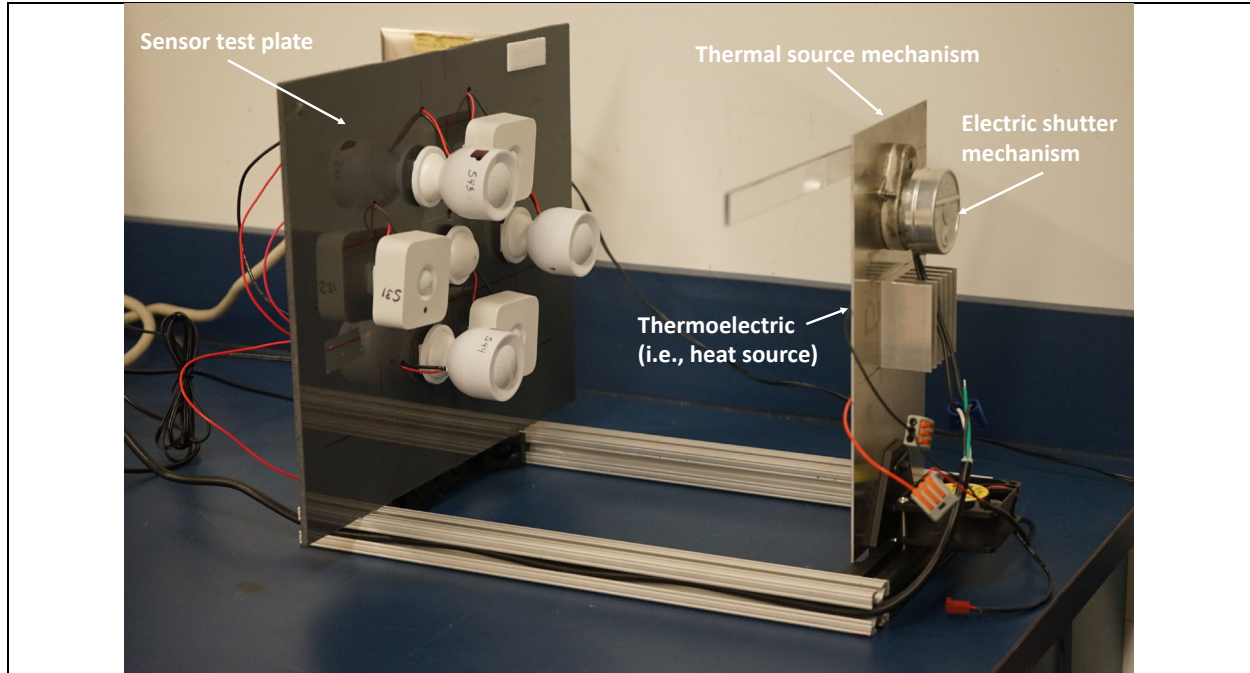
Figure 2-4. The continuous sensor test apparatus (CSTA)

3 Characterization of PIR Occupancy Sensors

3.1 NEMA Protocol

The NEMA protocol provides a set of definitions, measurement methods, and guidelines relevant to characterizing the horizontal (*x-y*) and vertical (*x-z*) FOV and coverage of occupancy, vacancy, and motion sensors [8]. The NEMA protocol requires that all testing be conducted indoors in a room (70 degrees Fahrenheit (°F) ± 5°F; 35–70% relative humidity [RH]) that is larger than the expected FOV of the sensor. The temperature, RH, room dimensions, and floor surface material are recorded as part of the testing report. The test area is subdivided into 3-foot (ft) × 3-ft cells, and the ability of the sensor to detect a human test subject in a cell is recorded. The sensor DUT is mounted as per the manufacturer's instructions and allowed to stabilize (the mounting height and any special instructions should be recorded). To characterize the DUT's performance, the testing is subdivided into major and minor motion testing. Major motion testing involves the movement of a person walking briskly through the test area (for more details, see **Section 3.1.1**). Minor motion testing describes the movement of a person sitting at an office desk and performing common motions such as reaching for a phone, turning the pages in a book, or opening a file folder (for more details, see **Section 3.1.2**).

3.1.1 Major Motion Testing in the NEMA Protocol

During major motion testing, the test subject (with a height of 67 ± 4 inches and a weight of 170 ± 20 pounds [lbs]) must have his or her head and hands exposed and must be wearing a shirt, long pants, and shoes. The test subject should not wear additional insulating garments (e.g., coat) or hanging or swaying material. These characteristics define the thermal profile of the test subject, and an example is given in **Figure 3-1**.
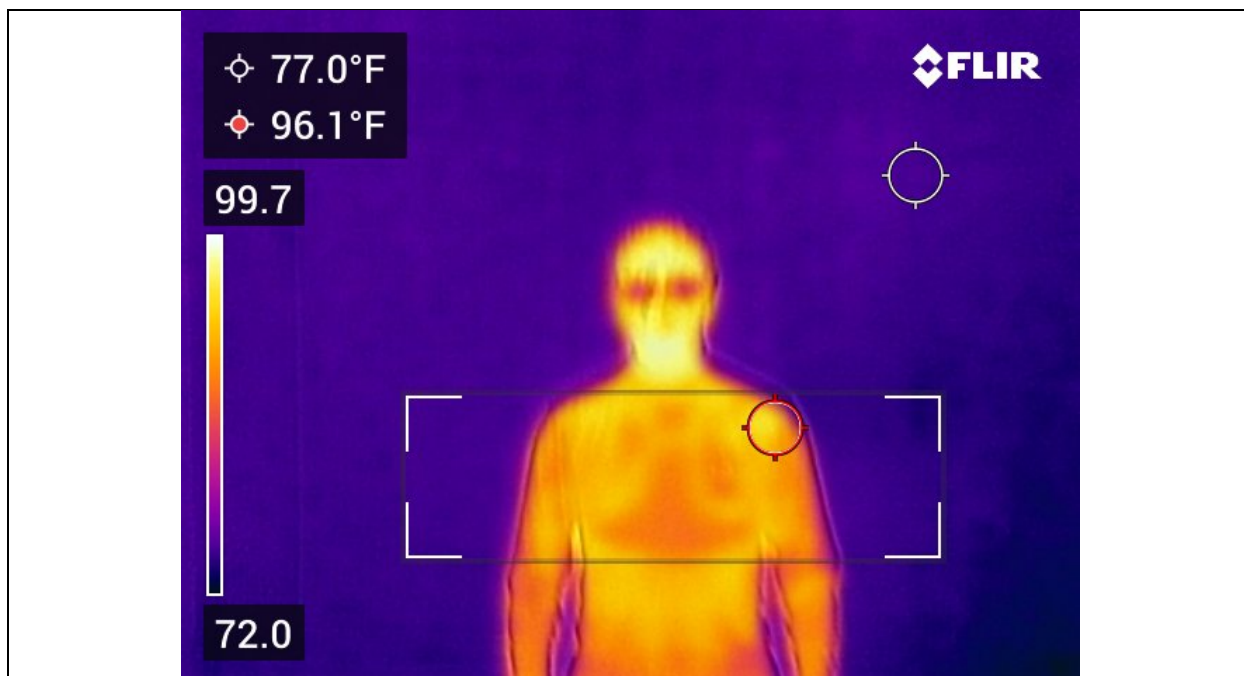
Figure 3-1. Thermal profile of a typical test subject meeting the requirements of the NEMA protocol for occupancy sensors

The test subject starts outside of the sensor's FOV and walks to the edge of the first cell at a rate of 4 ± 0.5 feet per second (ft/s).[*] The test subject shall walk methodically in a direction parallel to the surface of a sensor (i.e., y-direction) or a direction that is perpendicular to the surface of the sensor (x-direction). According to the NEMA protocol, the test subject must walk to the edge of the first cell, pause 2 s to note sensor response, and then proceed to the next cell. This process must be continued until the sensor's FOV is mapped in the x-direction, y-direction, or both. Results are recorded in a grid such as the one shown in **Figure 3-2**. The entire FOV can be tested when the sensor is centrally located and there is enough open space (ideally 35 ft or more) on either side of the sensor. Because the FOV of the sensors being tested requires a large room for testing, half of the FOV can be tested at a time by moving the sensor to opposite ends of the grid.

---

[*] During testing, the walking rate of 4.0 ± 0.5 ft/s was found to be a brisk pace and was subject to a large amount of variation if this pace was not monitored. Because the sensor detection distance appears to be influenced by walking speed, this experimental parameter could affect test results when using human test subjects but can be easily controlled with a mobile platform..

Figure 3-2. Example of the horizontal FOV of a PIR sensor

3.1.2 Minor Motion Testing in the NEMA Protocol

During the minor motion test in the NEMA protocol, a robotic arm (measuring 3 inches × 3 inches × 15 inches is placed at the center of a cell at a set height and moved at a fixed velocity. If motion is detected during a sweep of the robotic arm in a cell, then the cell is considered to be positive for minor motion, and the next cell is tested.

3.2 Revised NEMA Protocol and Evaluation Methods

Two principal methods were used to evaluate the reliability of the PIR occupancy sensors after accelerated stress test (AST) exposure. The first method determined whether the AST environment caused a change in the detection length of each DUT, which would be an indication of a parametric change. This test was quick to perform because it recorded detection distance only along the *x*-axis and was used to evaluate sensor reliability at intermediate times during the AST. The second method was a full sensor FOV test conducted according to the NEMA protocol; this test also provided information about parametric performance of the sensors. This FOV test was more time consuming and was only conducted on the test populations at the beginning and end of AST.

3.2.1 Determination of Sensor Triggering

A critical element of evaluating a sensor's performance was determining when the sensor detected motion sufficient enough to trigger a response. Theoretically, the full lighting system shown in **Figure 2-1** could be used to monitor triggering. When using this approach, activation of the sensor would cause a signal to be sent via WiFi to the system controller, which would then activate the appropriate switch to turn on the light. Unfortunately, this approach was found to have significant latency between triggering and lamp activation (> 1 min in some cases) for the products that were being tested, which created confusion about when the sensor was triggered and increased test times.

To overcome the issue of system latency, several different approaches were investigated. One obvious approach was to measure the output of the PIR sensor, but, in practice, the readings were somewhat difficult to interpret because of the bipolar nature of the PIR response and the impact of the associated electronics in the sensor. After a thorough investigation, it was decided to use the status of the indicator LED as a signal that the sensor had been triggered. When the sensor products examined in this report detected motion, an indicator LED turned on for a brief period (< 10 s). This response was found to occur almost instantaneously with the test subject entering the FOV of the PIR element. During the tests described in this report, activation of the indicator LED was visually monitored by the testing engineer, and the response was recorded for each test cell as required in the NEMA protocol. In addition to providing faster and more reproducible results, relying on the

sensor's indicator LED to signal sensor activation also eliminated the need for a controller and smart lamp in the testing setup. When the controller was used in the test system, only a single sensor could be studied at a time, but without the controller and relying only on the indicator LED for each sensor, it is possible to multiplex the sensors during testing. As a result, by relying on the indicator LED to denote sensor triggering status, multiple PIR sensors were simultaneously tested by arraying them on the test stand and watching for the response of each sensor as the test subject moved into each cell.

3.2.2   Detection Length Test

The DLT provided a simple measurement of the maximum distance at which the PIR sensor could detect the test subject. These tests were conducted in an open room with the DUT mounted at a height of 5 ft, and the sensor was located 2 ft from an adjoining wall. The temperature of the room was set to 71°F ± 4°F, and the RH was 62%. The flooring in the test area was linoleum tile. The test subject starts outside the FOV of the sensor at a distance of 36 ft along the *x*-direction and between 9 ft and 12 ft along the *y*-direction. The test subject then walks toward the line perpendicular to the surface of the sensor (i.e., the *x*-axis) along the *y*-direction (i.e., the test subject walks parallel to the surface of the sensor) until reaching the *x*-axis (i.e., the test subject is directly in front of the sensor at a distance of 36 ft). The test operator would pause for at least 10 s to see whether the sensor was triggered (i.e., the indicator LED was on). If the sensor was not triggered in this cell, then the test subject would exit the cell by moving in the *y*-direction, move 3 ft closer (e.g., 33 ft along the *x*-direction), and repeat the parallel movement motion until they were directly in front of the sensor again.

3.2.3   Horizontal FOV Test in an Open Room

Horizontal FOV tests were conducted in a large, open room by using both human subjects and RoboSES. The room had carpeted floors, and the ambient temperature was within the 70°F ± 5°F specified in the NEMA protocol. All testing with human subjects followed the NEMA protocol with two exceptions. The first exception was that the test subjected moved continuously from outside the sensor's FOV to a target cell instead of moving cell-by-cell as described in the NEMA protocol. This modification was chosen because past experience showed that the speed of motion was more likely to vary more in the cell-by-cell method than in the method where the test subject walks directly to a target cell. Second, we did not have staff within the height *and* weight requirements set forth by NEMA. In general, our staff used during initial testing fit the height *or* weight requirement.

When conducting the horizontal FOV tests, the sensor DUTs were mounted on a metal plate located on a detector stand on one side of the room. All chairs and furniture were moved to the edge of the room, as shown in **Figure 3-3**. The open area of the room was divided into a 3-ft × 3-ft grid as stated in the NEMA protocol. Because there are 100 different 3-ft × 3-ft cells in the test area, the total test area size was 30 ft × 30 ft. Because the detector stand was located at one corner of the test area, only one quadrant (i.e., 90 degrees) of the sensor's FOV is measured at a time. For simplicity, the sensor FOV is assumed to be symmetrical.

To avoid the possibility of unwanted variability that could arise because of DUT position on the stand, the DUTs were mounted in the same position and orientation during repeat FOV testing. Indicator markings on the exterior of the DUTs were used to confirm the placement and orientation matched the arrangement in the initial test.
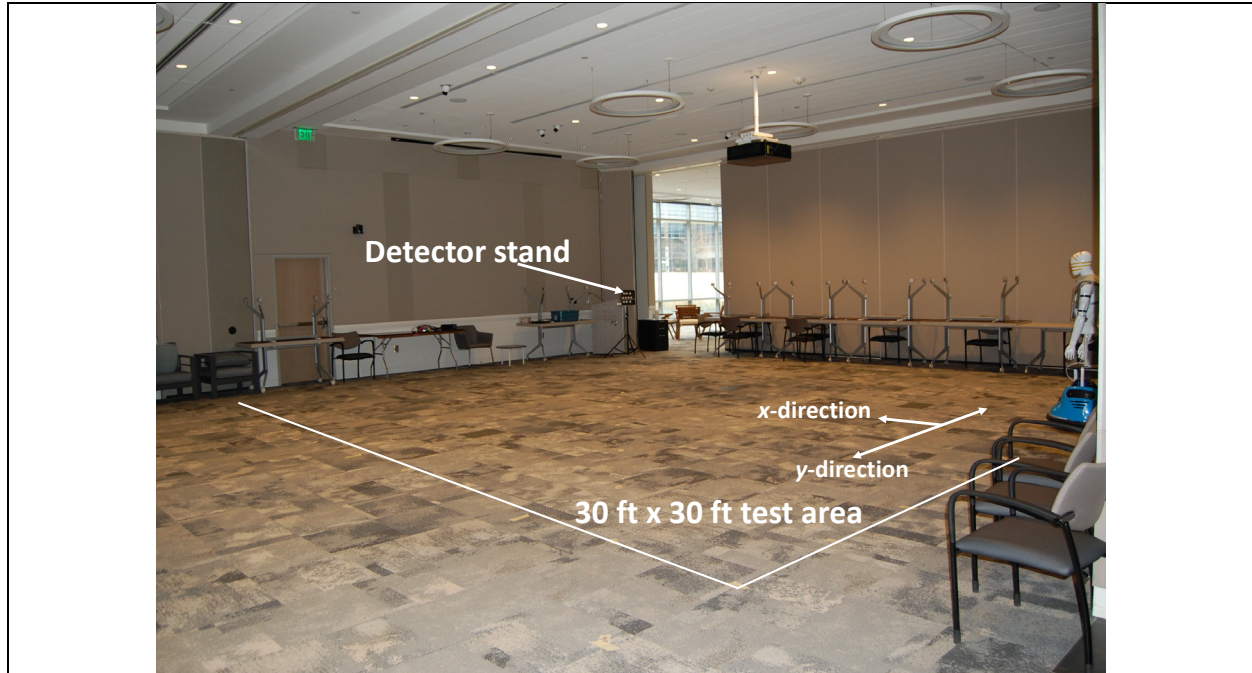
Figure 3-3. Large, open conference room and the grid layout used for the horizontal FOV tests

When conducting the test, the test subject would position himself or herself well outside the 30-ft × 30-ft test area because this allowed sufficient space to get up to the 4.0 ± 0.5 ft/s walking rate set forth in the NEMA protocol. The test subject would move at this rate to the target cell and stop for 10 s. If the sensor responded, as indicated by its LED, the cell was marked positive for major motion. Then, the test subject returned to the perimeter of the test area, and the test was restarted on another cell. Testing was initially conducted in the direction parallel to the surface of the sensor (i.e., the *y*-direction), and then was conducted in the direction perpendicular to the surface of the sensor (i.e., the *x*-direction).

4 Results

The PIR sensors examined during this study were characterized by using a combination of human and robotic test subjects. RoboSES was developed to increase test speed and improve test reproducibility. As shown in **Figure 4-1**, RoboSES consisted of two components: (1) a lower half featuring a motion base that can be driven remotely by an operator and (2) an upper half consisting of a mannequin torso with various thermal pads placed to emulate a human heat emission profile. The upper half (mannequin torso with thermal pads) and lower half (motion base) can be disconnected for ease of transportation to the site where sensor testing will occur. Additional information about RoboSES, including a bill of materials, is presented in **Appendix A** of this report.
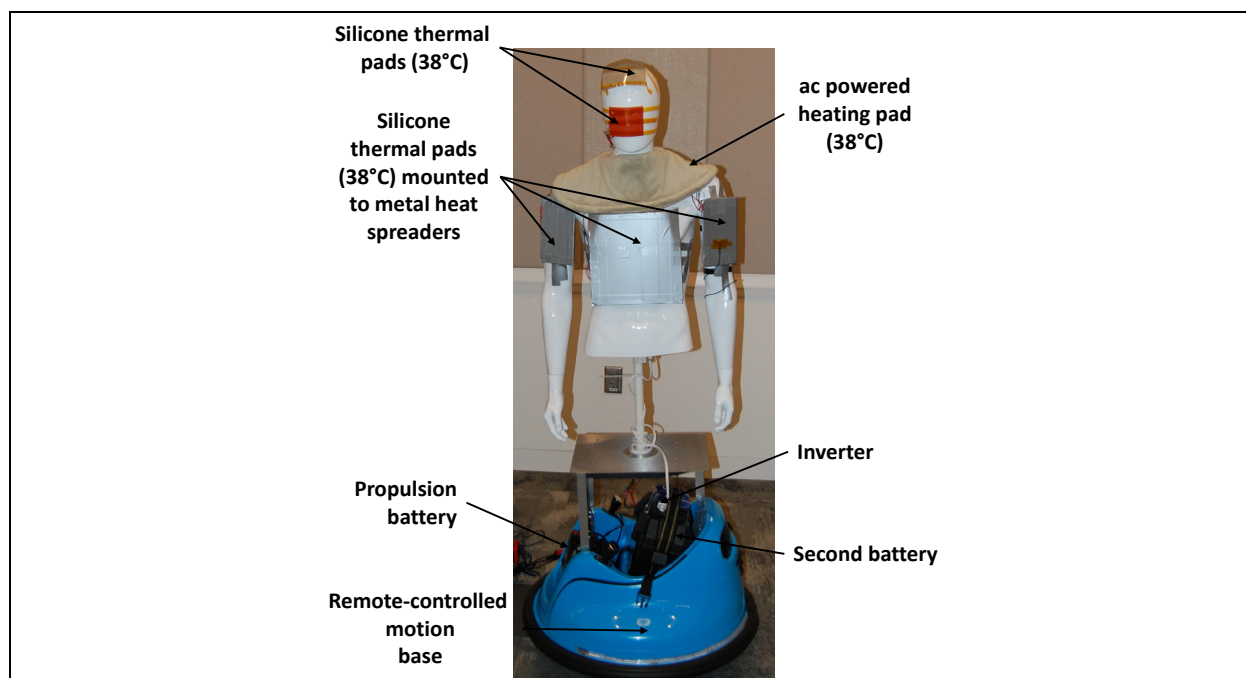
Figure 4-1. Final design of RoboSES for use in PIR sensor testing

Note: ac = alternating current.

4.1 Optimization of RoboSES

Designing RoboSES required testing a variety of configurations of direct current (dc)–powered silicone thermal pads (STPs) and alternating current (ac)–powered heating pads on the plastic mannequin torso. All electrical power to the heaters was supplied through two lead acid batteries, and the power consumption from the heaters and the battery capacity determined the maximum testing time before recharges. A commercial heating pad, powered from a battery through an inverter, was used to provide a gross temperature profile, and placement of the heating pad at different locations around the neck, chest, and abdomen were examined before deciding on a neck location. STPs were used as much as possible because of the lower power requirements and finer temperature control of these heaters. The placement of the thermal elements (i.e., STPs and heating pad) was optimized through an iterative process using IR imagery and comparing test results obtained with the NEMA protocol using both human and RoboSES test subjects. The final configuration of RoboSES is shown in **Figure 4-1** and its thermal profile is shown in **Figure A-1** in **Appendix A**. During the iterative design process, it was found that the STPs function better (i.e., provided a uniform thermal profile and required less energy use) when they are mounted on aluminum heat spreaders and are covered with duct tape. The use of duct tape helped to provide more uniform IR emission from the upper chest and arms and reduced the impact of heat reflections observed in thermal imaging. STPs were also mounted directly on the face and on top of the head without heat spreaders. The temperatures of the STPs were regulated by a controller and set to 38°C (± 2°C). The temperature of the heating pads was also set to 38°C and was controlled by the inner circuitry of the heating pad.

When optimizing the design for RoboSES, thermal sources were added at various locations on the robot's torso until the detection distance was approximately equal for a human subject and RoboSES. The average detection distances measured for five different samples of OS-1 and OS-2 (before any AST exposures) are presented in **Table 4-1** and **Table 4-2**, respectively, for a human test subject and for different configurations of RoboSES. Only the configuration shown in **Figure 4-1** was able to provide repeatable consistent results between the robotic and human test subjects. This configuration of RoboSES was used during DLT after AST exposure (see **Section 4.2**); however, RoboSES was found to lack the battery lifetime needed to perform the

FOV tests on the sample matrix used in this study. Accordingly, FOV measurements were taken with a human test subject with RoboSES serving as a backup.

Table 4-1. Detection Distance Results with OS-1

Test Subject	Experimental Protocol	Average Detection Distance (ft)	Repeated Measure (ft)
Human	NEMA protocol	27.0 (3.0)	27.2 (1.6)
RoboSES-1	Thermal pads on the face and hands only	9.3 (2.7)	8.4 (1.3)
RoboSES-2	Thermal pads added to chest	13.2 (1.6)	13.0 (1.7)
RoboSES-final	Final version of RoboSES	29 (1.7)	

Table 4-2. Detection Distance Results with OS-2

Test Subject	Experimental Protocol	Average Detection Distance (ft)	Repeated Measure (ft)
Human	NEMA protocol	25.8 (1.6)	24.6 (1.3)
RoboSES-1	Thermal pads on the face and hands only	12.6 (1.3)	15.0 (2.1)
RoboSES-2	Thermal pads added to chest	18.0 (3.0)	20.0 (1.7)
RoboSES-final	Final version of RoboSES	30 (0)	

4.2 Detection Length Test of AST Samples

The DLT was performed on all samples from RTOL, 55OL, and the rapid triggering ASTs. Measurements were taken on all DUTs when new (i.e., before any AST was performed) and at regular intervals for the duration of the test. For RTOL and 55OL, the test duration was 4,000 hrs, whereas the test duration was 2,000 hrs for the rapid triggering test. The results of the tests are presented in **Table 4-3** for both OS-1 and OS-2. The initial test results are reported for a human test subject because RoboSES underwent further optimization after the initial test. The final test results are provided only for RoboSES. Based on the results from the DLT tests, the sensors demonstrated good robustness, as evidenced by the finding that there was no significant change in the detection distance for any of the samples.

Table 4-3. DLT Results for OS-1 and OS-2 in Initial Condition and After AST

Test	OS-1		OS-2	
	Initial Distance	Final Distance	Initial Distance	Final Distance
Human	30 ± 0 ft	30 ± 0 ft	30 ± 0 ft	30 ± 0 ft
RTOL	29 ± 1.7 ft	30 ± 0 ft	30 ± 0 ft	29 ± 1.7 ft
55OL	29 ± 1.7 ft	30 ± 0 ft	28 ± 3.5 ft	29 ± 1.7 ft
Rapid trigger	27 ± 0 ft	30 ± 0 ft	28 ± 1.7 ft	29 ± 1.7 ft

4.3 FOV Test of AST Samples

FOV testing was performed in the large, open conference room shown in **Figure 4-1** by using human test subjects. RoboSES was unable to be used for most of the FOV testing because the battery lifetime was too short to allow completion of the test for all samples; therefore, only human test results are presented in this analysis. The room temperature was set to 70°F ± 3°F during all tests, and the flooring material was carpet.

The sensors were measured when they were new (i.e., initial measurement) and again at the end of the various ASTs. For simplicity, the average readings for all new samples were averaged together and are presented in this report. The average readings for the test populations from RTOL, 55OL, and rapid triggering tests were measured at the end of those tests and are also reported.

The FOV of the two sensor products was somewhat different as shown by the representative examples of the horizontal FOV results are presented in **Appendix B**. The coverage area FOV could be calculated by counting the number of 3-ft × 3-ft cells where motion was detected when using the NEMA protocol. During this analysis, the number of active cells was determined for the quadrant of the sensors' FOV that was measured. Knowledge of the FOV in this quadrant was sufficient for this analysis because the FOV is assumed to be symmetrical. The number of active 3-ft × 3-ft cells is presented in **Table 4-4** for each test condition.

Table 4-4. Number of Active Cells in the Tested Quadrant for FOV Test Results for OS-1 and OS-2 When the Sensors Were New and After AST[a]

Test	OS-1	OS-2
Initial FOV	51.1 ± 2.4	37.8 ± 5.2
4,000 hrs RTOL	49.3 ± 0.6	41.7 ± 0.6
4,000 hrs 55OL	49.3 ± 1.5	41.0 ± 1.7
2,000 hrs Rapid trigger	49.3 ± 1.5	40.7 ± 8.7

[a] The numbers given are the averages and standard deviations for DUTs in RTOL, 55OL, and the rapid triggering tests. For the initial FOV measurements, the average and standard deviation are calculated from nine DUTs.

A one-factor analysis of variance (ANOVA) was conducted on the population averages for OS-1 under the four test conditions. The ANOVA demonstrated that there was not a statistically significant difference in the means ($p = 0.416$) between the four populations of OS-1 (i.e., initial condition; after 4,000 hrs of RTOL; after 4,000 hrs of 55OL; and after 2,000 hrs of rapid triggering). The test findings are graphically illustrated by the boxplot chart for the data presented in **Figure 4-2**. The coefficient of variation[†] (CV) for the number of active cells was found to be small (< 5%) for all test populations of OS-1. This finding has three implications. First, each OS-1 sensor has a relatively consistent coverage area FOV (although there are some minor differences between the sensors as shown in **Appendix B**). Second, because the sensor's FOV is relatively uniform, the NEMA protocol test provides consistent results for OS-1. Third, in agreement with the DLT results, there is not a statistically significant change in the FOV for OS-1 after the different AST environments. These findings in aggregate suggest good robustness for these sensors against environment stressors in an indoor environment.

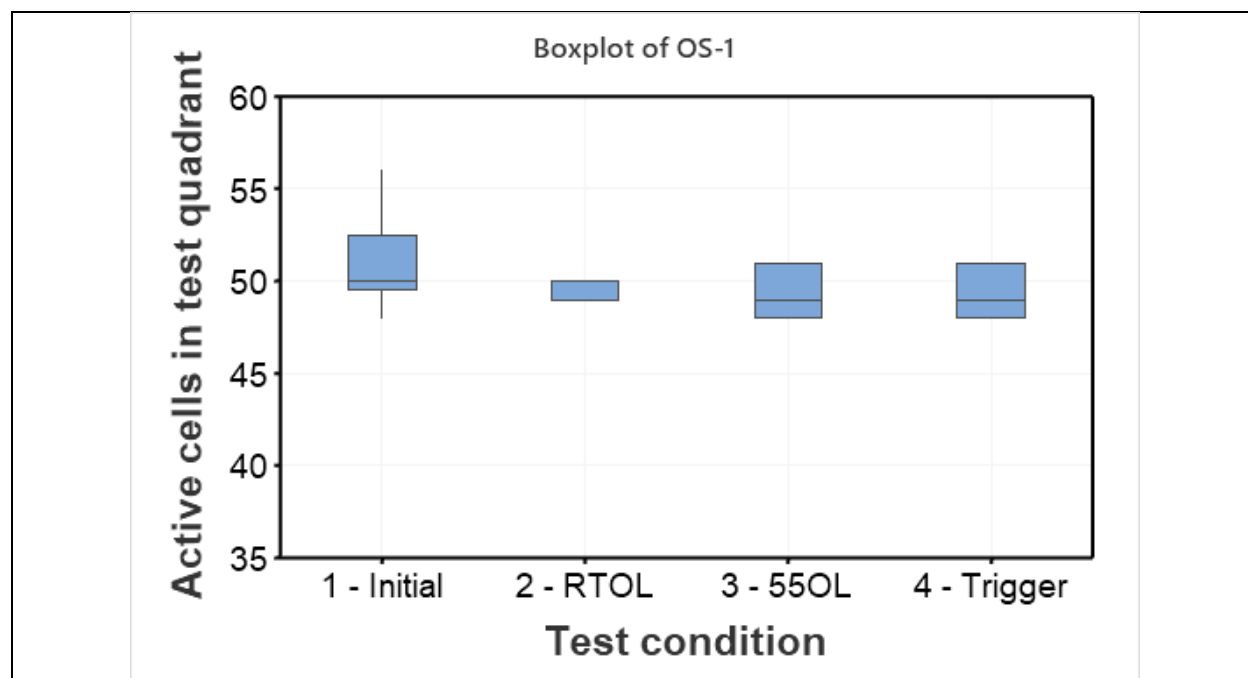[†] The "CV" is defined as the standard deviation divided by the mean.

Figure 4-2. Boxplot of the number of active cells in the test quadrant for the sample populations in the four test conditions for OS-1

However, when comparing the results for OS-2, the same level of consistency was not found. This finding is reinforced by the boxplot of the FOV area in the test quadrant, which is shown as **Figure 4-3**, and the comparison of the means and standard deviations presented in **Table 4-4**. Although the means of the OS-2 populations in the different tests varied by as much as 10%, the large variation in readings between different DUTs, even in the initial state, rendered the difference in means to be statistically insignificant ($p = 0.181$) as determined by a one-factor ANOVA. The largest CV value found for OS-2 was 21.5% for the rapid triggering measurements, and the next largest CV value was 17% for the initial test of all sensors. In contrast, the RTOL and 55OL test populations had relatively small CVs of 1.4% and 4.2%, respectively. Several conclusions can be drawn from these findings. First, the FOV of OS-2 was consistently smaller than the FOV of OS-1. Second, the number of active cells in the FOV varied widely for each OS-2 DUT, a point that is further confirmed by examination of the FOV plots in **Appendix B**. Finally, no statistical differences between the test populations of OS-2 were observed; however, in contrast to the findings for OS-1, the number of active cells in the FOV determined by the NEMA protocol for OS-2 DUTs varied greatly, implying large part-to-part variation. Identification of any small changes because of aging for OS-2 DUTs was therefore practically impossible.
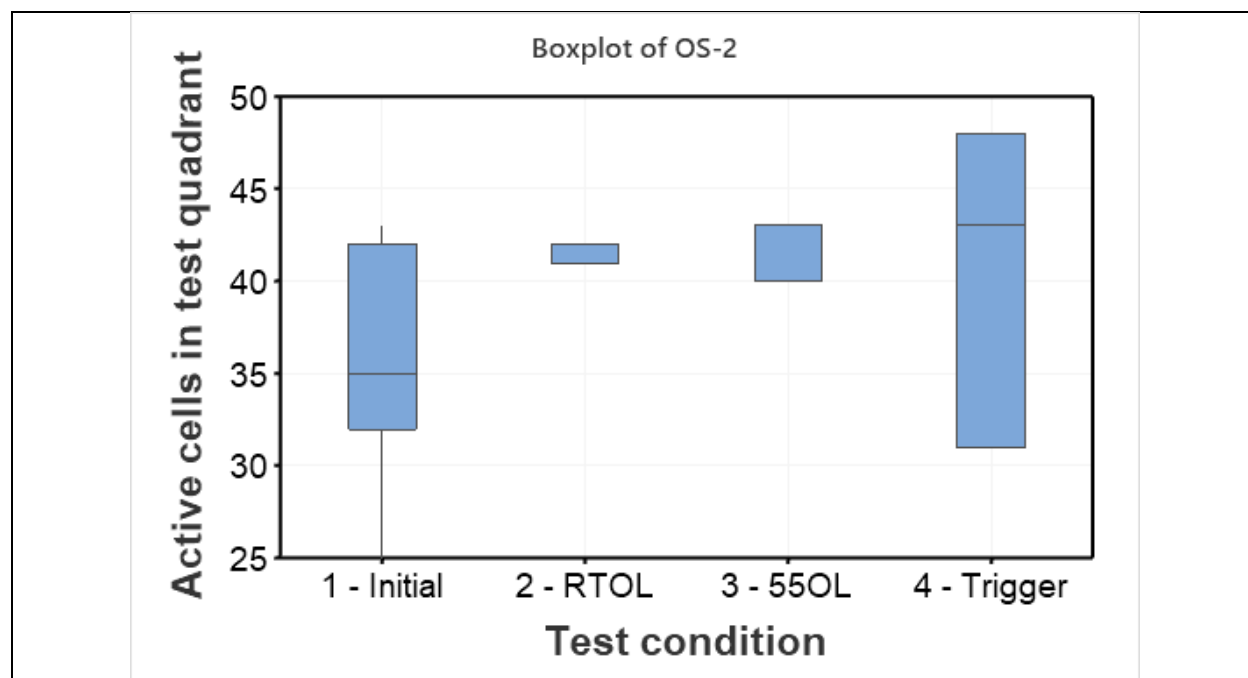
Figure 4-3. Boxplot of the number of active cells in the test quadrant for the sample populations in the four test conditions for OS-2

5 Discussion

The past decade has reinforced that there are significant opportunities for energy savings in general illumination by using SSL technologies based on LED sources [1]. The energy savings attributable to SSL technologies have been driven mainly by improvements in source efficiency, and luminous efficacy values of greater than 100 lumens per watt (lm/W) are now available from many lamp and luminaire product types as evidenced by the Design Lights Consortium's (DLC's) technical requirements for SSL products [14]. Although the gains in source efficiencies achieved by using LEDs have been significant, the inherent properties of LED sources, including instant on, easy dimmability, and rapid response to control signals, make this technology more amenable to lighting controls than many conventional sources. As a result, over the next 15 years, the use of lighting controls is expected to grow significantly, driven by LED technologies. In 2017, the annual energy savings from lighting controls in the United States was estimated as 0.6 quads; this amount of annual energy savings is expected to more than double to 1.3 quads by 2035 if DOE's lighting research program goals are met and the connected LCSs experience significant market penetration [1]. This energy avoidance is equivalent to an annual savings of more than $10 billion [1].

For lighting controls to deliver this level of energy savings, it is important for their reliability to be comparable to the remainder of the lighting systems. If the failure rate of lighting controls is higher than the remainder of the lighting systems, then the actual energy savings will not reach the projected levels. Therefore, it is just as important to understand the reliability of sensor systems that comprise lighting controls as it is to understand the reliability of the lighting products themselves.

The current report describes the performance of two commercial occupancy sensor products intended for use in residential applications. Separate populations of these products were tested as received and following their exposure to three different AST environments (i.e., RTOL, 55OL, and rapid triggering). Each population contained three devices, and separate populations were used for each AST environment. The maximum test temperature (55°C) was set by the typical maximum operating temperature of the PIR sensor and PE lens in these devices. Through 4,000 hrs of continuous operation in RTOL and 55OL, no statistically significant

differences in detection distances and coverage area FOV were found between the initial measurements and the post-AST measurement in any test environment. In addition, no statistically significant changes in detection distance and horizontal coverage area FOV were observed after the rapid triggering tests. These findings demonstrate that these products are robust, at least when tested to the limits of the ASTs that were used. Although the results for OS-1 were relatively consistent throughout (CV < 5%), demonstrating that the measurement methods used were sound, there was more variation in the measurements for OS-2 (CV up to 21.5%). This finding suggests greater part-to-part variability for OS-2 than OS-1. Such variability increases the difficulty in performing reliability tests because reliability and lifetime studies require repeated measurements on the same parts.

In the early days of SSL technology, the study of reliability drew heavily from previous work conducted in the electronics industry. In particular, the importance of identifying the appropriate metrics for reliability studies was emphasized, and the use of overstress testing was promoted as an important tool to identify design flaws and manufacturing defects [15]. Because most sensor technologies are derived from advancements in electronics technology and electronics packaging, a similar approach is likely the best method for evaluating the reliability of sensors used in SSL technologies.

However, one key difference between the LED lamps and luminaires used in lighting systems and the sensors used in LCSs is that an established testing infrastructure, complete with testing standards, existed very early in the development of commercial LED sources, but the situation is less clear for lighting sensors. Standards for testing SSL devices have been developed by several organizations, with the Illuminating Engineering Society (IES) being at the forefront in North America. The development of standards led the lighting industry to develop and support the consensus standards (e.g., American National Standards Institute [ANSI]/IES LM-79, ANSI/IES LM-80) that are widely used today for conducting tests on key metrics for lighting [16, 17]. These tests provide methods to consistently measure the key metrics of LEDs, lamps, and luminaires over time; this information is important in understanding the long-term performance and reliability of LED devices.

In contrast, the standards landscape for sensors used in lighting systems is less clear. NEMA took a leadership role by developing the NEMA protocol to measure the FOV of occupancy sensors based on PIR, ultrasonic, and microwave technologies. This testing protocol has helped to systematize the way in which information is collected about the basic performance of these types of sensors under ideal conditions in a manner analogous to the role that ANSI/IES LM-79 played in standardizing data acquisition for LED sources. Using the NEMA protocol, a large degree of part-to-part variability was demonstrated in some occupancy sensor products, which not only impacts their coverage area, but also increases the difficulty of performing reliability studies at the sensor level. The NEMA protocol is also often time consuming and costly to implement, which limits its utility as a regular measure of sensor degradation. To overcome this issue, the DLT test, which is derived from the NEMA protocol but not part of the test procedure in the NEMA protocol, was used. Other quick tests are also likely to be useful in sensor reliability studies. Consensus-based standard methods for performing such low-cost tests on sensors are needed for reliability testing on these devices.

Performing reliability testing on a population of sensors requires not only low-cost measurement techniques that can be quickly and repeatably performed on the sensor, but also protocols to accelerate aging of the sensors without changing the failure modes. Although the current work demonstrated good sensor robustness through 4,000 hrs of testing, more aggressive protocols are needed to produce measurable change in the sensors in a reasonable test period. More aggressive ASTs would involve higher temperatures than used here, higher humidities, or both. Another potential source of sensor reliability concern that may occur if germicidal ultraviolet (UV) systems become widespread is the impact of prolonged exposure of ceiling-mounted sensors to UV radiation, which could change the FOV of the Fresnel lens or impact the mechanical integrity of the polymer housing. Increasing the magnitude of environmental stressors may exceed the manufacturer's design limits and create new failure modes that are not likely to occur during normal usage. Consequently, additional research is needed to ensure that enhanced ASTs produce the proper aging acceleration without creating new failure modes.

Another critical question when evaluating the reliability of sensors used in the LCS is determining whether the test should be conducted at the sensor level or the whole system level. Regarding the residential do-it-yourself systems that were tested, it was found that the system latency was too high to perform a practical system test using the NEMA protocol. Instead, the status indicator LED was relied upon to show whether the sensor had been triggered. Most likely, other sensor systems will have lower latency, and tests may be possible at the system level, but that was not the case with the two systems examined during the current study. This finding of long latency in the full system associated with the PIR sensors examined in this report underscores the importance of understanding the limitations of the testing procedures to be used, as well as the limitations of the devices under test when performing any reliability study.

6 Conclusions

This report examines reliability testing of two commercially available sensors intended for use in the residential market. Separate populations of the sensors were subjected to one of three ASTs (i.e., RTOL, 55OL, or rapid triggering) that are intended to emulate typical use conditions anticipated by the manufacturer. The horizontal FOV of the sensors were evaluated by using the NEMA protocol (i.e., NEMA WD 7-2011 [R2016]). A DLT was used as a quick measure of an any changes in sensor detection distance in a direct line with the sensor. These tests demonstrated that no statistically significant change occurred in sensor performance after any of these ASTs when compared with the initial condition. This finding suggests that occupancy sensors are robust to changes in operating environment that typically occur indoors. Because no failure modes were identified due to environmental factors, it may be necessary to use higher environmental stressors (e.g., temperature, humidity, UV radiation). Such conditions would require additional research to ensure that new failure modes are not created.

References

1. Yamada, M., Penning, J., Schober, S., Lee, K., & Elliott, C. (2019, December). *Energy savings forecast of solid-state lighting in general illumination applications.* Prepared for the U.S. Department of Energy Lighting R&D Program. Retrieved from https://www.energy.gov/sites/prod/files/2019/12/f69/2019_ssl-energy-savings-forecast.pdf

2. U.S. Department of Energy. (2022, February). *2022 Solid-state lighting R&D opportunities.* Prepared for the U.S. Department of Energy Lighting R&D Program. Retrieved from https://www.energy.gov/sites/default/files/2022-02/2022-ssl-rd-opportunities.pdf

3. 360 Market Updates. (2018, February 20). *Global occupancy sensor market—Segmented by network type (wired, wireless), technology (ultrasonic, passive infrared, microwave), building type (residential, commercial), application, and region: Growth, trends and forecasts (2018–2023)*. Retrieved from https://www.360marketupdates.com/global-occupancy-sensor-market-12883821

4. Steiner, J. O. (2017). Conventional IR and ultrasonic sensor systems. Pp. 465–513 in Karlicek, R., Sun, C.-C., Zissis, G., & Ma. R. (Eds.). *Handbook of Advanced Lighting Technology.* Springer: New York.

5. Mukhopadhyay, B., Srirangarajan, S., & Kar, S. (2018). Modeling the analog response of passive infrared sensor. *Sensors and Actuators A, 279*, 65–75.

6. Feagin, Jr., B., Poplawski, M., & Day, J. (2020, August). *A review of existing test methods for occupancy sensors.* Prepared for the U.S. Department of Energy Lighting R&D Program. Retrieved from https://www.energy.gov/sites/prod/files/2020/08/f77/ssl-cls-review-test-method-occupancy-sensor-aug2020.pdf

7. Oljaca, M. (2020). *Techniques for PIR-based motion detection*. Retrieved from https://www.ti.com/lit/ml/slyp722/slyp722.pdf?ts=1645984662782&ref_url=https%253A%252F%252Fwww.ti.com%252Ftool%252FTIDA-00489

8. NEMA (National Electrical Manufacturers Association). (2016). *NEMA standards publication WD 7-2011 (R2016): Occupancy motion sensors standard*. Retrieved from https://www.nema.org/standards/view/occupancy-motion-sensors-standard

9. Panasonic Industry. (2021). *PIR motion sensor*. Retrieved from https://www.panasonic-electric-works.com/cps/rde/xbcr/pew_eu_en/ca_pir_motionsensors_1192_en.pdf.

10. MuRata. (n.d.). *Sensor IRA-S210ST01 data sheet*. Retrieved from https://www.murata.com/~/media/webrenewal/products/sensor/infrared/datasheet_pir.ashx?la=en

11. Duracell Battery. (n.d.). *OP1500 AA product data sheet*. Retrieved from: https://www.duracell.com/wp-content/uploads/2016/03/OP1500_US_OP1.pdf

12. Energizer Battery. (n.d.). *E91 product data sheet*. Retrieved from https://data.energizer.com/pdfs/e91.pdf

13. Eveready Battery. (n.d.). *Eveready 1215 product data sheet*. Retrieved from https://data.energizer.com/pdfs/1215.pdf

14. Design Lights Consortium. (2020, June). *Solid-state lighting (SSL) technical requirements version 5.1.* Retrieved from https://www.designlights.org/our-work/solid-state-lighting/technical-requirements/ssl-v5-1/.

15. Next Generation Lighting Industry Alliance and LED Systems Reliability Consortium. (2014, September). *LED luminaire lifetime: Recommendations for testing and reporting.* Third Edition. Retrieved from https://www.nglia.org/pdfs/led_luminaire_lifetime_guide_sept2014.pdf

16. ANSI (American National Standards Institute) and IES (Illuminating Engineering Society) (2019). *ANSI/IES LM-79-19: Approved method: Optical and electrical measurements of solid-state lighting products*. New York, NY: IES.

17. ANSI (American National Standards Institute) and IES (Illuminating Engineering Society) (2020). *ANSI/IES LM-80-20: Approved method: Measuring luminous flux and color maintenance of LED packages, arrays, and modules*. New York, NY: IES.

Appendix A

A-1. Robotic Test Vehicle

The Robotic Sensor Evaluation System (RoboSES), which was developed during this work, is an automated, remote-control device specifically designed to aid in the testing of passive infrared (PIR) occupancy sensors. RoboSES consisted of two components: a lower half featuring a motion base that can be driven remotely by an operator and an upper half consisting of a mannequin torso with various thermal pads placed to emulate a human heat emission profile. The upper half (mannequin torso with thermal pads) and lower half (motion base) can be disconnected for ease of transportation to site sensor testing locations. Bills of materials for the RoboSES are presented in **Table A-1**, **Table A-2**, and **Table A-3** of this appendix.

Designing RoboSES required testing a variety of configurations of direct current (dc)–powered silicone thermal pads (STPs) and alternating current (ac)–powered heating pads on the plastic mannequin torso. All electrical power to the heaters was supplied through two lead acid batteries, and the power draw from the heaters and the battery capacity determined the maximum testing time before recharges. A commercial heating pad, powered from a battery through an inverter, was used to provide a gross temperature profile, and placement of the heating pad at different locations around the neck, chest, and abdomen were examined before deciding on a neck location. STPs were used as much as possible because of the lower power requirements and finer temperature control of these heaters. The placement of the thermal elements (i.e., STPs and heating pad) was optimized through an iterative process using infrared (IR) imagery and comparing test results obtained with the only standard available. The National Electrical Manufacturers Association (NEMA) developed the standard, NEMA WD 7-2011 (R2016), to test occupancy and motion sensor performance (herein referred to as "the NEMA protocol"). Hence, the NEMA protocol was used to test the human and the RoboSES test subjects. The final configuration of RoboSES is shown in **Figure 4-1**, and its thermal profile is shown in **Figure A-1**. During the iterative design process, it was found that the STPs function better (i.e., provided a uniform thermal profile and required less energy use) when they are mounted on aluminum heat spreaders and are covered with duct tape. The use of duct tape helped to provide more uniform IR emission from the upper chest and arms and reduced the impact of heat reflections observed in thermal imaging. STPs were also mounted directly on the face and on top of the head without heat spreaders. The temperatures of the STPs were regulated by a controller and set to 38 degrees Celsius (°C; ± 2°C). Although this temperature is slightly above human body temperature (36.1°C to 37.2°C), this setting helped increase the response reproducibility for RoboSES by ensuring that the set temperature did not go below human body temperature. The temperature of the heating pads was set to 38°C and was controlled by the inner circuitry of the heating pad.

Figure A-1. Thermal profile of RoboSES when in operation

The motion base of RoboSES houses much of the necessary hardware to simulate a human test subject for occupancy sensor testing. At its core, RoboSES uses a commercially available, 12 volt dc (V_{dc}) electric bumper car, which is equipped with Bluetooth for remote control driving. The original, 12 V_{dc} battery (for operating the bumper car) remained housed under the black seat plate in the center of the base system. A scaffolding system was added to the bumper car to mount the upper half of the mannequin, as shown in **Figure 4-1.** A second lead acid battery was mounted to the top of the black seat plate of the bumper car, and this battery powered the STPs, heating pad, and other auxiliary functions. RoboSES operates at a consistent speed of 3.6 ft/s, which meets the requirements of the NEMA protocol. RoboSES can be driven forward or backward and can spin 360 degrees (to assist in navigation). When RoboSES is used during an occupancy sensor test, an operator drives the electric bumper car to the cells set forth by the NEMA protocol—just like a human subject would walk through the cells. Automated control through a series of grid patterns on the floor can be added in the future to improve the speed and accuracy of testing. We found that RoboSES provides fast and reproducible readings for the DLT. Unfortunately, the battery capacity of RoboSES was not sufficient for it to be used in full horizontal FOV measuring according to the NEMA protocol. Accordingly, only human measurements were used for horizontal FOV test.

A-2.   Major Components of RoboSES

RoboSES was constructed in two components to aid in moving the device to different locations for sensor testing. The two components are the lower motion base and heated upper torso as shown in **Figure A-2**. Consideration was made in the design to provide ease of use with simple connections from the power source to the heated upper torso and lower motion base. A list of the major components (aside from power considerations) for the lower motion base and heated upper torso are provided in **Table A-1** and **Table A-2**, respectively. The major power and hardware requirements for RoboSES are provided in **Table A-3**. The components listed in **Table A-1**, **Table A-2**, and **Table A-3** do not include small components (e.g., electrical connectors) that would be common in a laboratory space.
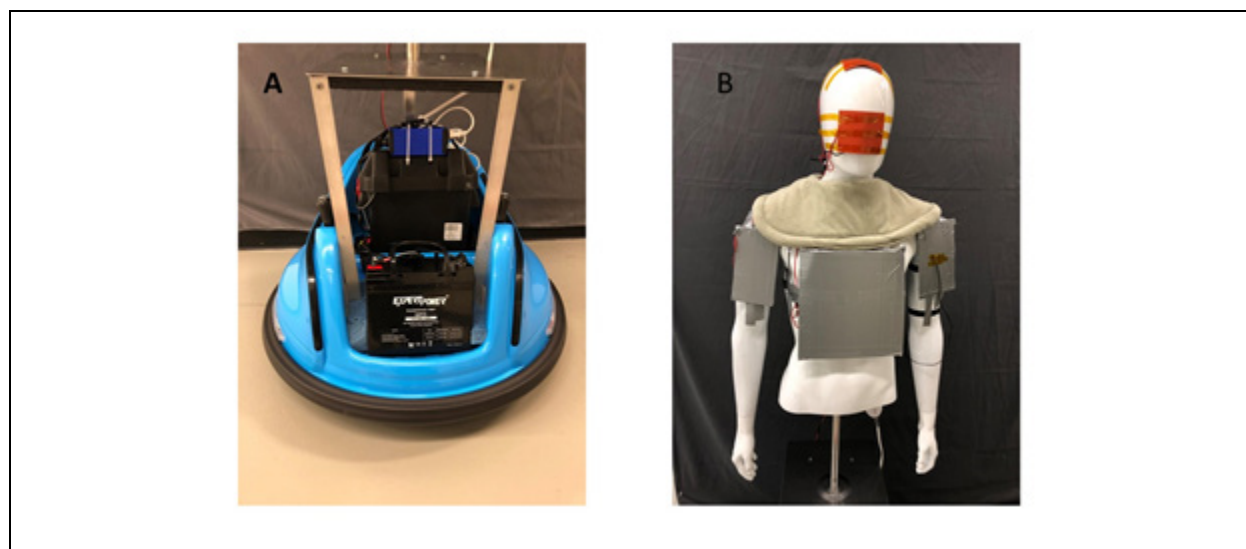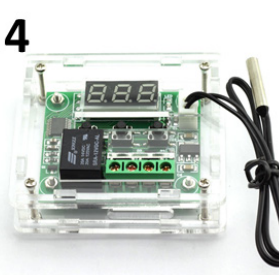

Figure A-2. The two components of the RoboSES: (A) the lower motion base and (B) the heated upper torso

Table A-1. Major Electronic Components in the Motion Base of RoboSES

ID	Component	Details	Quantity	Price/Unit ($)
1	Bumper car with remote control	360 spin, 12 V_{dc}, 2 speed, Bluetooth, weight limit 66 lbs	1	199.96
2	Photoelectric beam sensor (optional)	Normally open or normally closed switchable	1	19.99
3	Strobe siren red light (optional)	110 decibels at 12 V_{dc}	1	9.99

Note: lbs = pounds; V_{dc} = direct current volt.

Table A-2. Major Components of the Upper Half (Torso and Head) of RoboSES

ID	Component	Details	Quantity	Price/Unit ($)
4	Digital cooling/heating temperature controller	12 V_{dc}	5	9.99
5	Heating pad	22 × 19 inches	1	42.99
6	Thermal pads (pack of four)	12 V, 25 W, 80 mm × 100 mm	2	19.99
7	Male mannequin half body	Weight: 12 lbs	1	99.95

Note: lbs = pounds; mm = millimeter; V = volt; V_{dc} = direct current volt; W = watt.

Table A-3. Additional Power Needs and Hardware for RoboSES

ID	Component	Details	Quantity	Price/Unit ($)
9	Rechargeable battery	12 V, 35 Ah	2	64.99
10	Battery charger	12 V_{dc}, 2 A	2	31.39
11	Battery box	To safely hold a 12-V battery	1	14.29
12	Reflective tape	Silver, 2 inches by 20 ft	1	9.99
13	6061 Aluminum 90 degree angle	1/16-Inch wall thickness, 1-inch high × 1-inch wide	2	26.89
14	Pointed screws for plastic	410 Stainless steel, number 8 size, ¾-inch long	1	11.78
15	Wire	18 AWG, solid, 50–100 ft of two different colors (e.g., red, black)	2	11.84

Note: A = amp; Ah = amp-hour; AWG = American Wire Gauge; ft = feet; V = volt; V_{dc} = direct current volt.

Appendix B
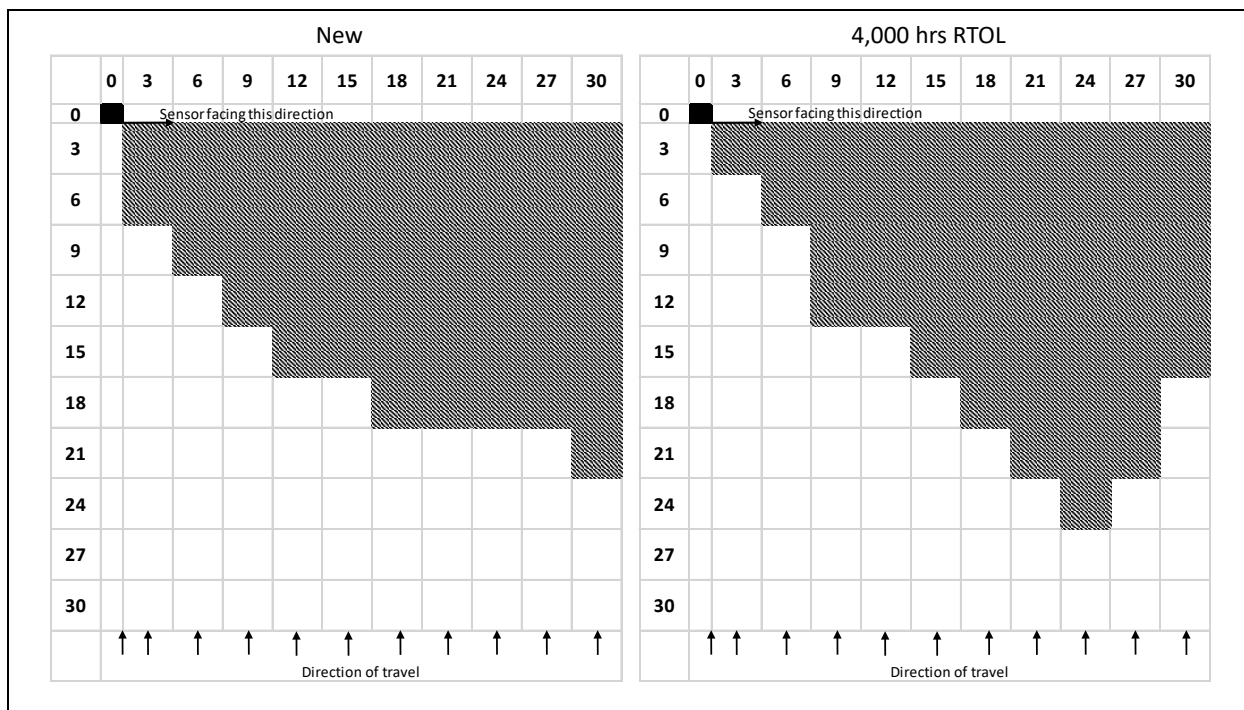
Figure B-1. Horizon field of view (FOV) of a representation Occupancy Sensor Number 1 (OS-1) device under test (DUT) when it was new and after 4,000 hours (hrs) of room temperature operating life (RTOL)
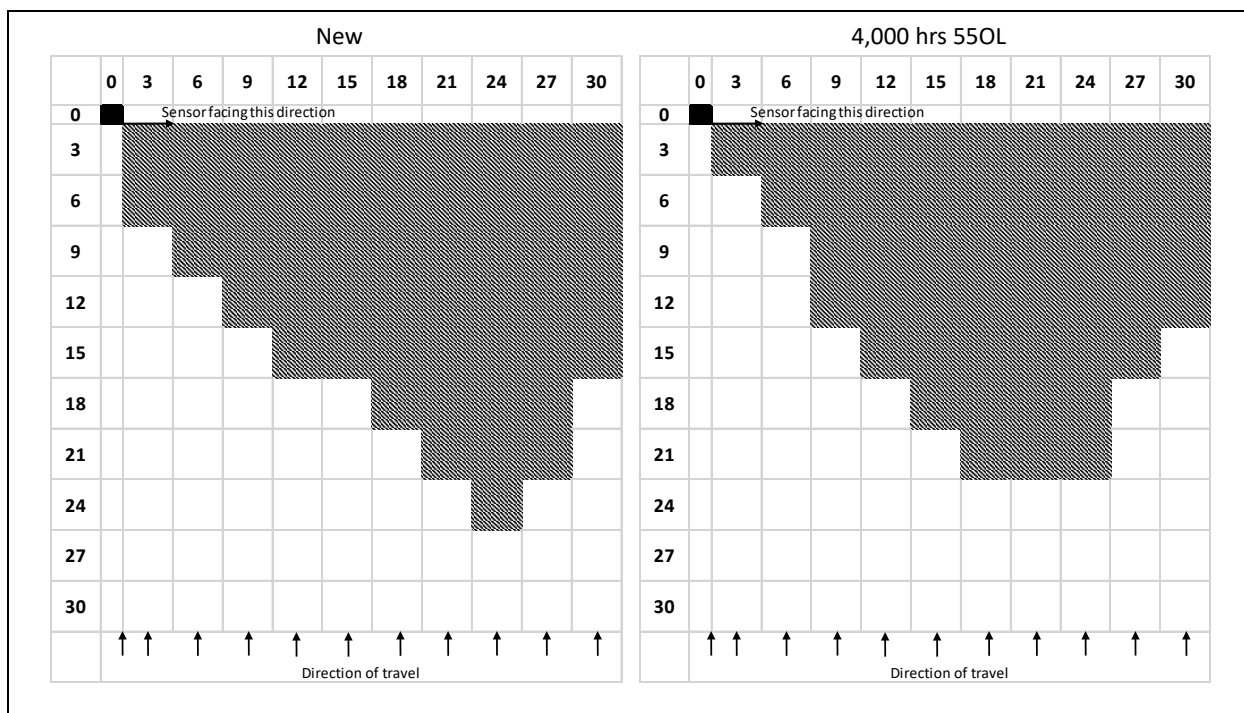

Figure B-2. Horizon FOV of a representation OS-1 DUT when it was new and after 4,000 hrs of operating lifetime tests conducted at 55 degrees Celsius (°C) (55OL)
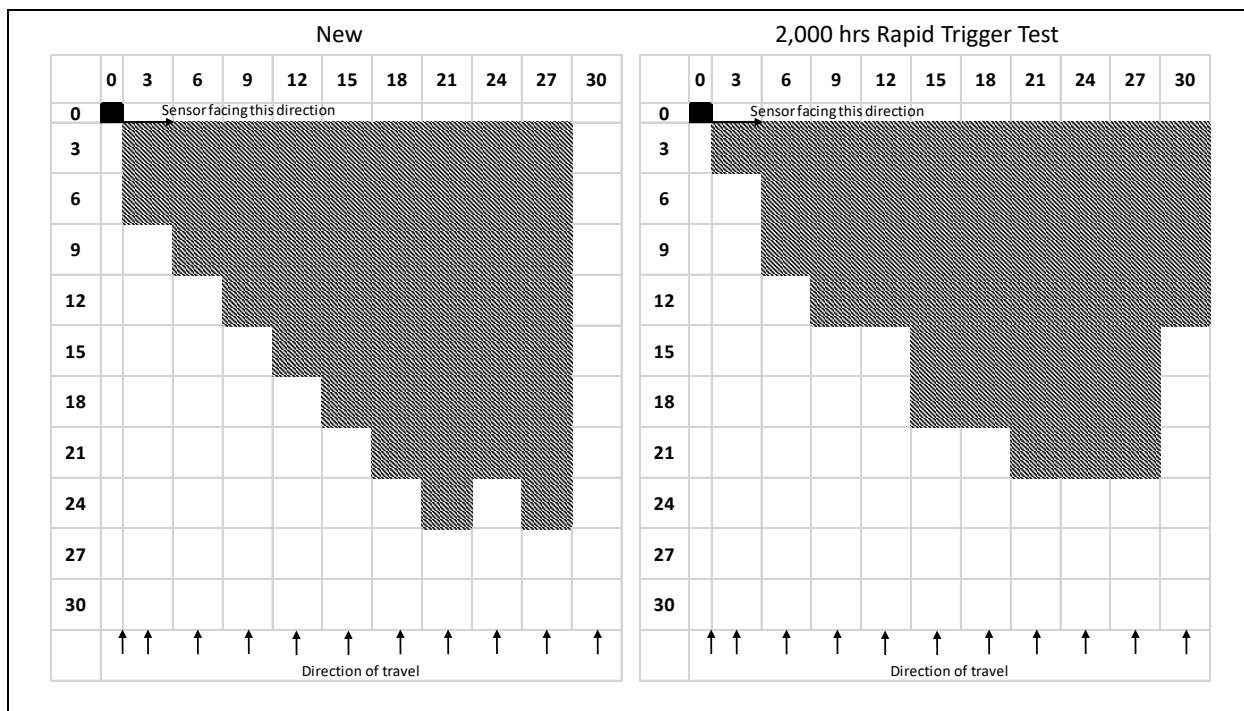
Figure B-3. Horizon FOV of a representation OS-1 DUT when it was new and after 2,000 hrs of rapid triggering test
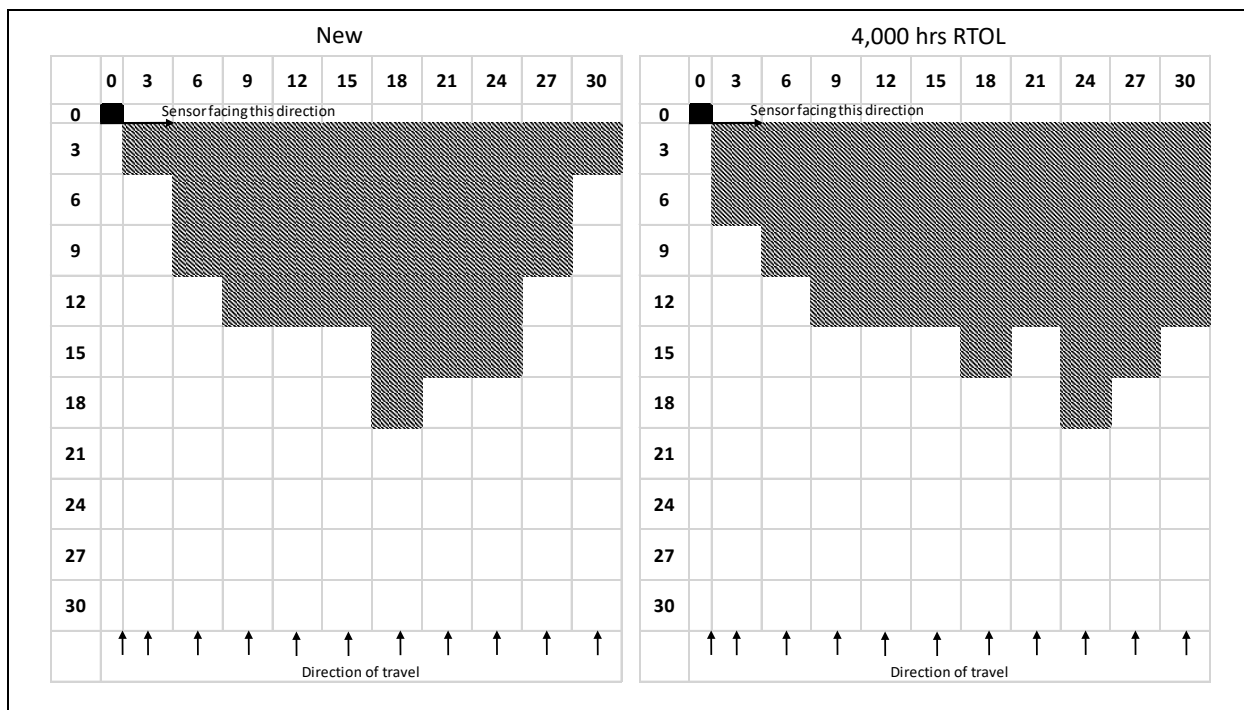

Figure B-4. Horizon FOV of a representation Occupancy Sensor Number 2 (OS-2) DUT when it was new and after 4,000 hrs of RTOL
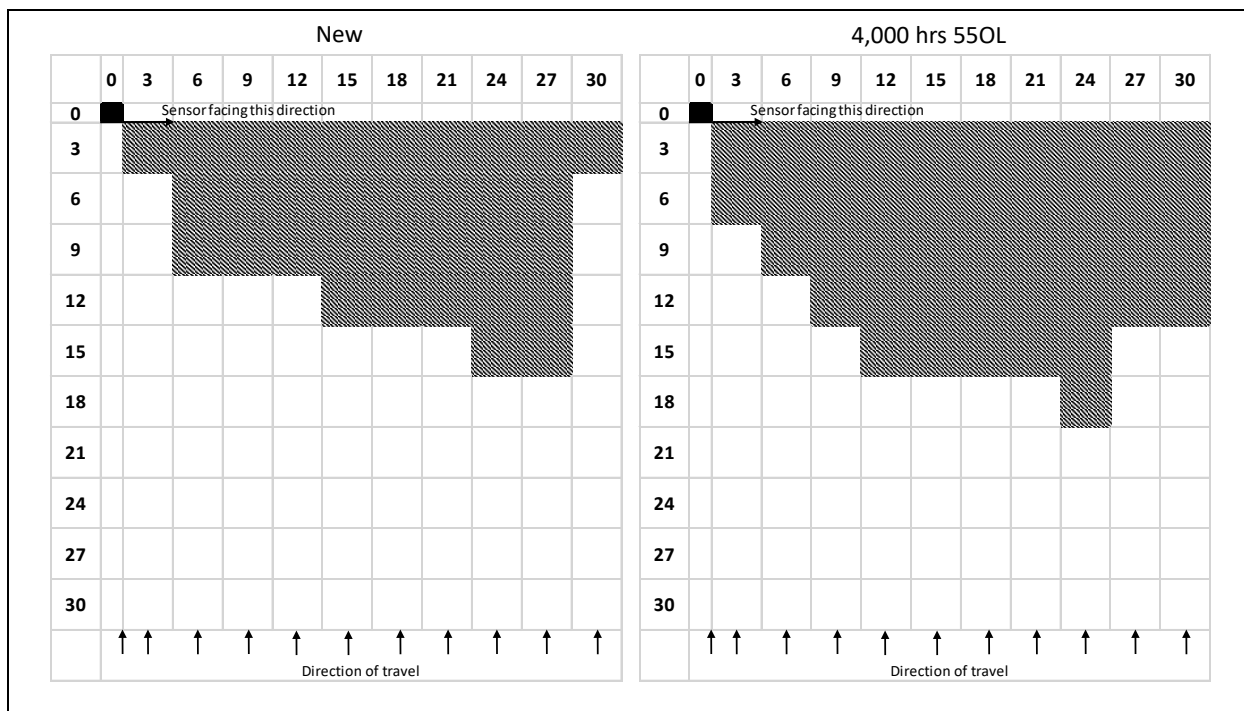
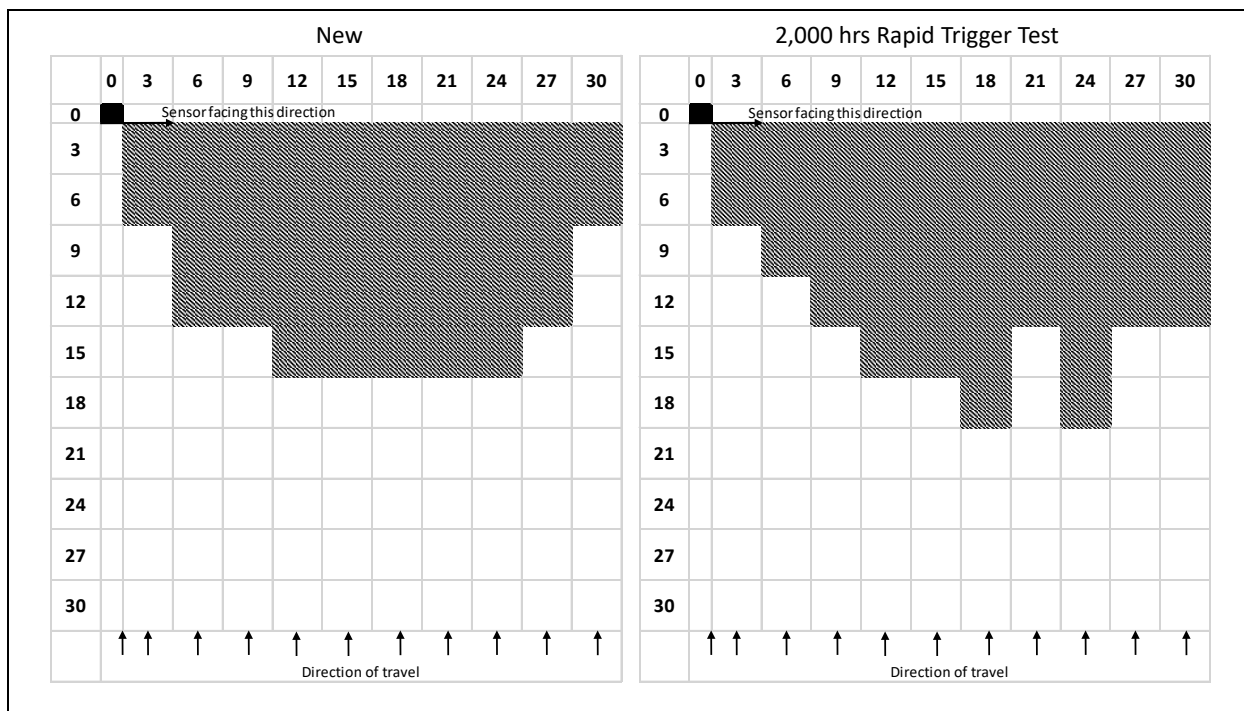Figure B-5. Horizon FOV of a representation OS-2 DUT when it was new and after 4,000 hrs of 55OL

Figure B-6. Horizon FOV of a representation OS-2 DUT when it was new and after 2,000 hrs of rapid triggering test